Available online at www.sciencedirect.com
SCIENCE DIRECT®
ELSEVIER
International Journal of Solids and Structures 43 (2006) 4297–4322
INTERNATIONAL JOURNAL OF SOLIDS and STRUCTURES
www.elsevier.com/locate/ijsolstr

Flexural–torsional buckling of misaligned axially moving beams. I. Three-dimensional modeling, equilibria, and bifurcations

Kevin Orloske [a], Michael J. Leamy [b], Robert G. Parker [a,*]

[a] *Department of Mechanical Engineering, Ohio State University, 650 Ackerman Road, Columbus, OH 43202, USA*
[b] *The MITRE Corporation, 7515 Colshire Dr., McLean, VA 22102, USA*

Received 8 March 2005
Available online 10 October 2005

Abstract

The equations of motion for the flexural–flexural–torsional–extensional dynamics of a beam are generalized to the field of axially moving continua by including the effects of translation speed and initial tension. The governing equations are simplified on the basis of physically justifiable assumptions and are shown to reduce to simpler models published in the literature. The resulting nonlinear equations of motion are used to investigate the flexural–torsional buckling of translating continua such as belts and tapes caused by parallel pulley misalignment.

The effect of pulley misalignment on the steady motion (equilibrium) solutions and the bifurcation characteristics of the system are investigated numerically. The system undergoes multiple pitchfork bifurcations as misalignment is increased, with out-of-plane equilibria born at each bifurcation. The amount of misalignment to cause buckling and the post-buckled shapes are determined for various translation speeds and ratios of the flexural stiffnesses in the two bending planes. Increasing translation speed decreases the misalignment necessary to cause flexural–torsional buckling. In Part II of the present work, the stability and vibration characteristics of the planar and non-planar equilibria are analyzed.

Keywords: Axially moving; Beam; Buckling; Stabililty; Flexural-torsional; Bifurcation

1. Introduction

The present work examines the mechanics of translating, beam-like continua that exhibit complex equilibria as a result of boundary misalignment. More specifically, this work considers beams of small aspect ratio for which the bending stiffnesses in two planes have large disparity, examples of which include belt drives, tape drives, and band saw blades. Under the action of boundary misalignment in the plane of larger bending

* Corresponding author. Tel.: +1 614 688 3922; fax: +1 614 292 3163.
E-mail address: parker.242@osu.edu (R.G. Parker).

0020-7683/$ - see front matter © 2005 Elsevier Ltd. All rights reserved.
doi:10.1016/j.ijsolstr.2005.08.014

stiffness, these axially moving beams experience flexural–torsional buckling into a three-dimensional post-buckled state.

The translating continuum model has direct application to automotive belt-pulley systems undergoing parallel pulley misalignment, where the center of one pulley is displaced in the plane of larger belt bending stiffness. Prediction of a threshold misalignment to cause buckling is necessary to establish tolerances for robust design. Similar boundary misalignment issues arise in tape drives and band saws.

Previous relevant research divides into three areas: flexural–torsional buckling of beams, three-dimensional equilibrium shapes of beams, and flexural–torsional buckling of translating beams. Of these, flexural–torsional buckling of stationary beams occupies the most literature. The present research does not consider thin-walled beams such as I-beams where cross-sectional warping becomes significant (Vlasov, 1961): flexural–torsional buckling of thin-walled beams occupies its own place in the literature (Trahair, 1993) and is not considered.

The first published works on flexural–torsional buckling known to the authors appeared in 1899 (Michell, 1899; Prandtl, 1899) for thin, rectangular, solid beams. Michell considers five different configurations and in each case neglects the bending curvature in the plane of greatest flexural rigidity prior to buckling. Because in each case the beam is loaded parallel to this plane, the effect of bending prior to buckling is neglected. Prandtl develops the same theory as Michell but generalizes it to include the first order effect of the principal bending curvature.

Hodges and Peters (1975) derive a general buckling equation that includes effects not considered by Michell and Prandtl. They then apply a first order approximation to the principal bending curvature and show the resulting buckling equations are actually simpler than those previously published. An historical review of the developments between Michell and Prandtl's work and that of Hodges and Peters is given in Reissner (1979), where transverse shear deformation is included. Milisavljevic (1995) considers the flexural–torsional stability of a cantilever in the presence of shape and load imperfections. Hodges (2001) considers flexural–torsional flutter instabilities that arise from a deep cantilever loaded by a lateral follower force at the tip.

In all works discussed, the flexural–torsional stability of specific systems is analyzed. Michell (1899) considers five systems, Timoshenko (1936) looks at several others, Hodges and Peters (1975) consider only a cantilever with a transverse end load, while Milisavljevic (1995) considers a cantilever with a simultaneous distributed force and an axial force. None include beam translation speed, pre-tensioning, or extension as considered herein. Even without these effects, however, the authors have not found published work on the configuration considered in the present work, namely buckling due to boundary displacement such as pulley misalignment.

Much of the literature on flexural–torsional buckling determines the buckling loads without exploring the three-dimensional shape of the buckled member. Raboud et al. (1996) determined various three-dimensional equilibrium shapes of an inextensible cantilever beam loaded by constant tip or uniform distributed loads. Multiple equilibria are found using a numerical shooting procedure. The potential energies of the post-buckled shapes are used to compare the configurations, but the local stability of each configuration is not addressed. Later, Raboud et al. (2001) examined the stability of the same system except only constant tip loads are considered.

The literature on translating beams is vast, but the literature on flexural–torsional buckling of translating beams is very sparse. The first work in this area was published by Mote (1968), who was motivated by the buckling of band saw blades under edge loads. He models the ends of the beam as simply supported and neglects flexure in the direction of loading. It is shown that transport velocity lowers the critical edge load. After this work little, if any, similar work was done in this area.

Other previous related research falls into the areas of axially moving beams and three-dimensional beam theories. The axially moving beam literature addresses mainly systems undergoing solely transverse or sometimes transverse-extensional motion. A translating beam theory that includes geometric and inertia nonlinearities arising from three-dimensional motion does not exist in the literature. For stationary beams in the absence of initial tension, Crespo da Silva and Glynn (1978) developed such a model for inextensible beams. This work was later generalized to extensible beams (Crespo da Silva, 1988). The three-dimensional translating beam theory developed in the present work further generalizes this model to include translation speed and initial tension. In addition, the present work applies a different reduction scheme than used in Crespo da Silva (1988) to simplify the equations of motion.

The present work focuses on system modeling, equilibria, and bifurcation behavior. After discussing the system and some underlying assumptions, the three-dimensional kinematics of a translating beam including geometric and inertia nonlinearities are discussed, followed by derivations of the strain energy and kinetic energy expressions. Hamilton's principle is used to obtain the equations of motion. The non-dimensional equations of motion are simplified on the basis of physically justifiable assumptions for the boundary conditions of interest. Next, equilibria are determined for changing misalignment. Planar equilibria are determined and characteristics of the bifurcation points are discussed. The effect of translation speed and flexural stiffness ratio on the bifurcation points is explored. Following discussion of the planar equilibria, the post-buckled out-of-plane equilibria are studied. In part II of this paper (Orloske and Parker, this issue), the equations of motion are linearized about an arbitrary equilibrium configuration and vibration and stability analysis of the equilibria are conducted.

2. Problem formulation

This work models a single span of a belt-pulley or band-wheel system such as occur in belt drives, tape drives, band saws, etc. The continuum is modeled as a translating beam. It is assumed that there is no interaction between the free span being modeled and the bounding pulleys. An example system is illustrated in Fig. 1. The $\mathbf{E}_1$ direction is along the centroidal axis of the undeformed free span. $\mathbf{E}_2$ is in the plane of the pulleys orthogonal to $\mathbf{E}_1$. $\mathbf{E}_3$ completes the right-handed orthonormal basis.

The general assumptions regarding the system are listed here, with more specific assumptions given were used later:

{1} The beam translation speed c remains constant before and after deformation.
{2} Prior to deformation, the tension T is constant and the beam is straight.
{3} The detachment and attachment points, points G and H in Fig. 1, are stationary during deformation.
{4} During deformation the beam does not slip on the pulleys.
{5} Gravitational acceleration, structural damping, and any interactions with the environment are neglected.

Assumption {2} must be explicitly stated because in actuality a continuum wrapping on pulleys has a small initial curvature in the $\mathbf{E}_1$–$\mathbf{E}_2$ plane and non-uniform tension due to axial translation and wrapping of a non-zero flexural stiffness medium about circular pulleys (Kong and Parker, 2003, 2005).

2.1. Kinematics

Let χ^r denote the reference configuration of the beam when the only deformation is due to initial tension. This configuration will also be referred to as the trivial equilibrium. χ^f denotes the final configuration of the beam. The beam translates in both configurations. The orthonormal triad $\mathbf{E}_i$ is centered at point G. Arclength

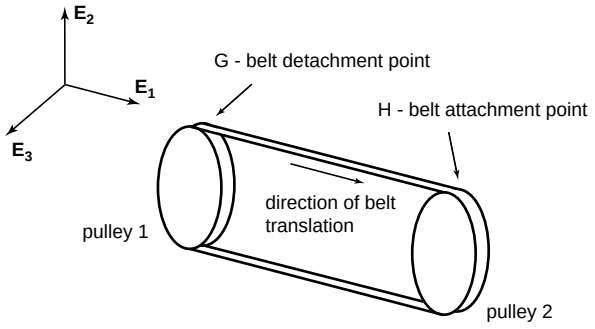

Fig. 1. An example of a belt-pulley system where the free span between points G and H represents an arbitrary free span in any belt-pulley system.

is measured along the beam's centroidal axis starting at point G. The arclength in the χ^r configuration is denoted by x and the arclength in the χ^f configuration is denoted by s.

Fig. 2 shows the beam in the χ^r and χ^f configurations. Consider a cross-section in χ^r parallel to the $\mathbf{E}_2$–$\mathbf{E}_3$ plane. The centroid of this cross-section is point M^r. The body-fixed Cartesian triad $\mathbf{e}_i$ is centered at M^r, and $\mathbf{e}_i$ aligns with $\mathbf{E}_i$ in χ^r. When deformation occurs, M^r displaces to point M^f. The components of this displacement with respect to $\mathbf{E}_1$, $\mathbf{E}_2$, and $\mathbf{E}_3$ are u, v, and w, respectively. The orientation of $\mathbf{e}_i$ with respect to $\mathbf{E}_i$ is obtained by three successive Euler angle rotations. The details of this transformation and the definition of the Euler angles are displayed in Fig. 3. Triads $\mathbf{l}_i$ and $\mathbf{m}_i$ are used only as intermediate triads for this transformation.

The following assumptions are made:

{6} Cross-sectional warping due to torsion is neglected.
{7} In-plane cross-sectional distortion, such as that arising from Poisson's ratio, is neglected.
{8} All cross-sections remain perpendicular to the beam centerline.

Assumption {6} is relaxed later in the development to account for the torsional rigidity of a non-circular cross-section. Assumptions {6} and {8} together imply that plane sections remain plane. Assumptions {6}, {7}, and {8} together imply that at each position along the centroidal axis the cross-section acts as a two-dimensional rigid body moving in three-dimensional space. The translation of a cross-section is given by u, v, and w, and the orientation is described by $\alpha = \psi$, ϕ, θ. Assumption {8} implies that rotation of the cross-section is due to bending and torsion alone. Consequently, the six degrees of freedom are not independent. Fig. 4 illustrates the following relationships between the first two Euler angle rotations and the components of displacement:

$$\tan\psi = \frac{v'}{1+u'}, \quad \tan\phi = \frac{-w'}{\sqrt{(1+u')^2+v'^2}} \tag{1}$$

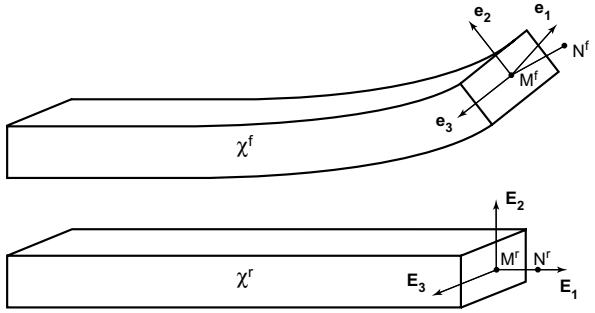

Fig. 2. Beam model in the χ^r and χ^f configurations. The right side is cut to show an arbitrary cross-section.

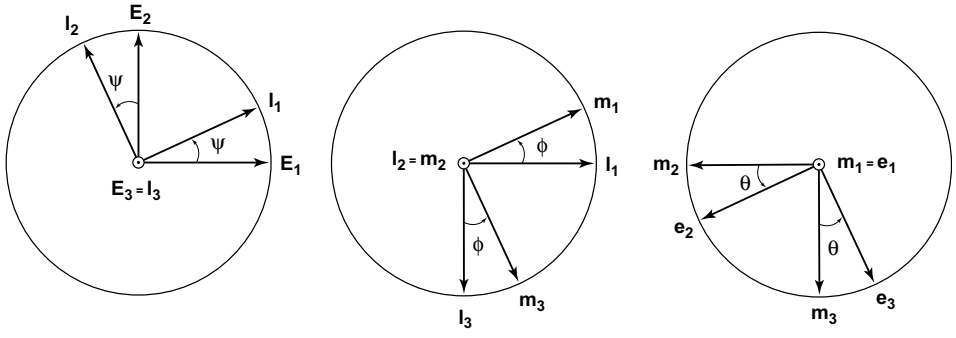

Fig. 3. Sequence of rotations (from left to right) that brings $\mathbf{E}_i$ into $\mathbf{e}_i$.

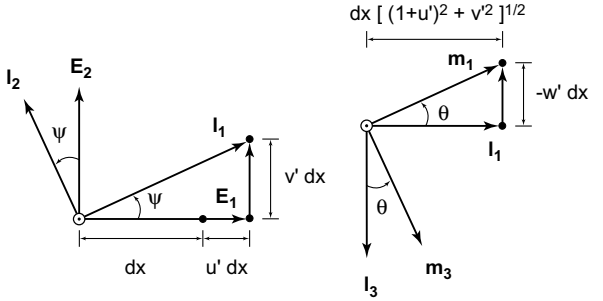

Fig. 4. Relation between rotations and displacement. The vectors $\mathbf{E}_i$, $\mathbf{l}_i$, and $\mathbf{m}_i$ are only used to illustrate direction and, only in this figure, are not necessarily unit vectors.

where prime denotes differentiation with respect to x. With these constraints there are four independent degrees of freedom at each position along the centroidal axis.

Consider the infinitesimal line segment M^{r} to N^{r} of length $\mathrm{d}x$ on the centroidal axis of the beam in Fig. 2. The position of N^{f} with respect to M^{f} is

$$\mathbf{r}_N = (\mathrm{d}x + u'\mathrm{d}x)\mathbf{E_1} + v'\mathrm{d}x\mathbf{E_2} + w'\mathrm{d}x\mathbf{E_3} \tag{2}$$

By definition, the length of the line segment M^{f} to N^{f} is $\mathrm{d}s$. Using this along with (2) gives

$$\frac{\partial s}{\partial x} = \sqrt{(1+u')^2 + v'^2 + w'^2}, \quad e_0 = \frac{\partial s - \partial x}{\partial x} = \sqrt{(1+u')^2 + v'^2 + w'^2} - 1 \tag{3}$$

where e_0 is the axial strain of the centroidal axis.

The angular velocity $\boldsymbol{\omega}$ at a given cross-section is

$$\frac{\mathrm{D}\mathbf{e}_i}{\mathrm{D}t} = \boldsymbol{\omega} \times \mathbf{e}_i \tag{4}$$

where $\mathrm{D}/\mathrm{D}t$ is the material derivative. Using Fig. 3 the angular velocity is

$$\boldsymbol{\omega} = (\dot{\psi} + \psi' c)\mathbf{E_3} + (\dot{\phi} + \phi' c)\mathbf{l_2} + (\dot{\theta} + \theta' c)\mathbf{e_1} = \omega_\xi \mathbf{e_1} + \omega_\eta \mathbf{e_2} + \omega_\zeta \mathbf{e_3} \tag{5}$$

where the dot denotes differentiation with respect to time. The convective velocity terms $\psi' c$, $\phi' c$, and $\theta' c$ result from the changing position x of a material particle and the material derivative, e.g., $\mathrm{D}\psi(x,t)/\mathrm{D}t = \dot{\psi} + \psi' c$. The components of $\boldsymbol{\omega}$ are

$$\begin{aligned}
\omega_\xi &= (\dot{\theta} + \theta' c) - (\dot{\psi} + \psi' c)\sin\phi \\
\omega_\eta &= (\dot{\psi} + \psi' c)\cos\phi\sin\theta + (\dot{\phi} + \phi' c)\cos\theta \\
\omega_\zeta &= (\dot{\psi} + \psi' c)\cos\phi\cos\theta - (\dot{\phi} + \phi' c)\sin\theta
\end{aligned} \tag{6}$$

Kirchhoff's kinetic analogy (Love, 1944) relating angular velocity to curvature is used to arrive at an expression for curvature. To invoke the analogy the convective terms in the material derivative are not included. This is equivalent to vanishing translation speed c, in which case the angular velocity $\hat{\boldsymbol{\omega}}$ is defined by

$$\frac{\partial \mathbf{e}_i}{\partial t} = \hat{\boldsymbol{\omega}} \times \mathbf{e}_i \quad \text{for } c = 0 \tag{7}$$

The components of $\hat{\boldsymbol{\omega}}$ on the $\mathbf{e}_i$ basis are

$$\begin{aligned}
\hat{\omega}_\xi &= \dot{\theta} - \dot{\psi}\sin\phi \\
\hat{\omega}_\eta &= \dot{\psi}\cos\phi\sin\theta + \dot{\phi}\cos\theta \\
\hat{\omega}_\zeta &= \dot{\psi}\cos\phi\cos\theta - \dot{\phi}\sin\theta
\end{aligned} \tag{8}$$

The curvature vector $\hat{\boldsymbol{\kappa}}$ of the centroidal axis is defined as

$$\frac{\partial \mathbf{e}_i}{\partial s} = \hat{\boldsymbol{\kappa}} \times \mathbf{e}_i \tag{9}$$

Using Kirchhoff's kinetic analogy the components of $\hat{\boldsymbol{\kappa}}$ on the $\mathbf{e}_i$ basis are obtained by changing the time derivatives in (8) to spatial derivatives. This gives

$$\begin{aligned} \hat{\kappa}_\xi &= \theta^+ - \psi^+ \sin\phi \\ \hat{\kappa}_\eta &= \psi^+ \cos\phi \sin\theta + \phi^+ \cos\theta \\ \hat{\kappa}_\zeta &= \psi^+ \cos\phi \cos\theta - \phi^+ \sin\theta \end{aligned} \tag{10}$$

where plus (+) denotes differentiation with respect to s and $\hat{\kappa}_\xi$, $\hat{\kappa}_\eta$, and $\hat{\kappa}_\zeta$ are components of $\hat{\boldsymbol{\kappa}}$. Using (3) and the chain rule in (10) gives

$$\begin{aligned} \kappa_\xi &= \theta' - \psi' \sin\phi \\ \kappa_\eta &= \psi' \cos\phi \sin\theta + \phi' \cos\theta \\ \kappa_\zeta &= \psi' \cos\phi \cos\theta - \phi' \sin\theta \end{aligned} \tag{11}$$

where

$$\kappa_\alpha = \hat{\kappa}_\alpha (1 + e_0) \quad \alpha = \xi, \eta, \zeta \tag{12}$$

By comparing (9)–(11), it is clear that (11) expresses the $\mathbf{e}_i$ components of a vector $\boldsymbol{\kappa}$ defined by

$$\frac{\partial \mathbf{e}_i}{\partial x} = \boldsymbol{\kappa} \times \mathbf{e}_i \tag{13}$$

The components of $\boldsymbol{\kappa}$ are not the traditional curvatures unless the beam is inextensible (Pai and Nayfeh, 1990), in which case $e_0 = 0$ and $\mathrm{d}s = \mathrm{d}x$. Traditional curvatures describe how the $\mathbf{e}_i$ basis changes with the arclength s of the current configuration. The curvatures needed in the remainder of this work describe how the $\mathbf{e}_i$ basis changes with the arclength x of the reference configuration.

2.2. Strain energy

Some additional assumptions are

{9} The strains are infinitesimal.
{10} The beam is a linear, elastic continuum.

Let point P^{r} be any material point on a given cross-section in the reference configuration and let ξ, η, and ζ denote the coordinates with respect to the body-fixed triad $\mathbf{e}_i$. When the beam deforms, P^{r} moves to P^{f}. Recall that in χ^{r}, $\mathbf{e}_i$ and $\mathbf{E}_i$ align, so the position of P^{r} relative to the detachment point (G in Fig. 1) is

$$\mathbf{r}^{\mathrm{r}}_{\mathbf{P}} = (x + ct)\mathbf{E_1} + \eta \mathbf{E_2} + \zeta \mathbf{E_3} \tag{14}$$

Assumption {6} is now relaxed and replaced with the following assumption:

{11} Cross-sectional warping due to torsion is neglected with the exception of its influence on the torsional rigidity.

Considering a static deflection for torsional rigidity purposes, P^{r} experiences a small axial displacement d due to warping. This displacement is modeled as

$$d\mathbf{e_1} = f(\eta, \zeta)\kappa_\xi \mathbf{e_1} \tag{15}$$

where $f(\eta, \zeta)$ is the warping function and κ_ξ is the $\mathbf{e_1}$ component of $\boldsymbol{\kappa}$. The displacement d exists because when a non-circular cross-section undergoes torsion, plane sections do not remain plane (Timoshenko and Goodier, 1970). As stated in assumption {11}, the sole purpose of including d is to account for the torsional rigidity of a

non-circular cross-section. To include this effect for a single purpose one must make assumptions to neglect other effects of axial warping. Eq. (15) is from the problem of static uniform torsion of prismatic bars and was solved by Saint-Venant (Timoshenko and Goodier, 1970). When torsion is not uniform along the prismatic continuum there are additional axial stresses due to local suppression of warping. These additional stresses produce a greater torsional stiffness than would be calculated by Saint-Venant's uniform torsion solution for the same κ_ξ (Ritchie and Leevers, 1999). If κ_ξ is not constant, (15) no longer holds at a given cross-section. This difference is ignored in this work. Hence, the torsional warping model is summarized by the following assumption:

{12} A Saint-Venant torsion model is used regardless of the axial variation of κ_ξ.

This implies that at a given cross-section, the beam's torsional cross-sectional warping is decoupled from bending and is from uniform torsion with a constant value of κ_ξ, where κ_ξ is the value at that cross-section.

With the above torsion model, the position of P^{f} relative to G is

$$\mathbf{r}^{\mathrm{f}}_{\mathbf{P}} = (x+u+ct)\mathbf{E_1} + v\mathbf{E_2} + w\mathbf{E_3} + f\kappa_\xi \mathbf{e_1} + \eta\mathbf{e_2} + \zeta\mathbf{e_3} \tag{16}$$

The Lagrangian finite strain tensor $\mathbf{L}$ is obtained using

$$d_t\mathbf{r}^{\mathrm{f}}_{\mathbf{P}} \cdot d_t\mathbf{r}^{\mathrm{f}}_{\mathbf{P}} - d_t\mathbf{r}^{\mathrm{r}}_{\mathbf{P}} \cdot d_t\mathbf{r}^{\mathrm{r}}_{\mathbf{P}} = d_t\mathbf{r}^{\mathrm{r}}_{\mathbf{P}} \cdot 2\mathbf{L} d_t\mathbf{r}^{\mathrm{r}}_{\mathbf{P}} \tag{17}$$

where $d_t\alpha$ is the differential of α holding time fixed. The differential elements are

$$d_t\mathbf{r}^{\mathrm{r}}_{\mathbf{P}} = \mathrm{d}x\mathbf{E_1} + \mathrm{d}\eta\mathbf{E_2} + \mathrm{d}\zeta\mathbf{E_3} \tag{18}$$

$$d_t\mathbf{r}^{\mathrm{f}}_{\mathbf{P}} = [(1+u')\mathbf{E_1} + v'\mathbf{E_2} + w'\mathbf{E_3}]\mathrm{d}x + \kappa_\xi\left(\frac{\partial f}{\partial \eta}\mathrm{d}\eta + \frac{\partial f}{\partial \zeta}\mathrm{d}\zeta\right)\mathbf{e_1} + \mathrm{d}\eta\mathbf{e_2} + \mathrm{d}\zeta\mathbf{e_3} + (f\kappa_\xi\mathbf{e}'_1 + \eta\mathbf{e}'_2 + \zeta\mathbf{e}'_3)\mathrm{d}x \tag{19}$$

Noting that the axial strain of the centerline ($\eta = \zeta = 0$) is in the $\mathbf{e}_1$ direction and using (3) yields

$$(1+u')\mathbf{E_1} + v'\mathbf{E_2} + w'\mathbf{E_3} = (e_0+1)\mathbf{e_1} \tag{20}$$

Use of (13) and (20) in (19) gives

$$d_t\mathbf{r}^{\mathrm{f}}_{\mathbf{P}} = \left[\frac{\partial f}{\partial \eta}\mathrm{d}\eta\kappa_\xi + \frac{\partial f}{\partial \zeta}\mathrm{d}\zeta\kappa_\xi + (e_0+1)dx\right]\mathbf{e_1} + \mathrm{d}\eta\mathbf{e_2} + \mathrm{d}\zeta\mathbf{e_3} + [(\kappa_\xi\mathbf{e_1} + \kappa_\eta\mathbf{e}_2 + \kappa_\zeta\mathbf{e}_3) \times (f\kappa_\xi\mathbf{e_1} + \eta\mathbf{e}_2 + \zeta\mathbf{e}_3)\mathrm{d}x] \tag{21}$$

Eqs. (18) and (21) are used on the left-hand side of (17), which is then factored to yield the following components of $\mathbf{L} = [\varepsilon_{ij}]$ with respect to the $\mathbf{E}_i \otimes \mathbf{E_j}$ basis

$$\begin{aligned}
&\varepsilon_{11} = e^* + \frac{1}{2}[(e^*)^2 + \kappa_\xi^2(\eta - f\kappa_\eta)^2 + \kappa_\xi^2(f\kappa_\zeta - \zeta)^2] \\
&\varepsilon_{22} = \frac{1}{2}\left(\frac{\partial f}{\partial \eta}\right)^2\kappa_\xi^2, \quad \varepsilon_{33} = \frac{1}{2}\left(\frac{\partial f}{\partial \zeta}\right)^2\kappa_\xi^2, \quad \varepsilon_{23} = \frac{1}{2}\frac{\partial f}{\partial \eta}\frac{\partial f}{\partial \zeta}\kappa_\xi^2 \\
&\varepsilon_{12} = \frac{1}{2}\kappa_\xi\left[(1+e^*)\frac{\partial f}{\partial \eta} + f\kappa_\zeta - \zeta\right] \quad \varepsilon_{13} = \frac{1}{2}\kappa_\xi\left[(1+e^*)\frac{\partial f}{\partial \zeta} + \eta - f\kappa_\eta\right]
\end{aligned} \tag{22}$$

where $e^* = e_0 + \zeta\kappa_\eta - \eta\kappa_\zeta$ is the axial strain of any line segment off the centerline. From assumption {9}, the strains are infinitesimal and it follows that e^*, $\kappa_\xi(\partial f/\partial\eta)$, and $\kappa_\xi(\partial f/\partial\zeta)$ are small. The strains are linearized in these quantities. As stated in {11}, f is only included to account for the torsional rigidity, and assumption {12} further states the torsional rigidity of interest is that which arises from a Saint-Venant torsion model. Since Saint-Venant torsion models pure torsion and not a combination of torsion and bending, the terms $f\kappa_\eta$ and $f\kappa_\zeta$ arising from coupled bending and torsion are removed in adherence to assumptions {11} and {12}. With these simplifications, (22) reduces to

$$\varepsilon_{11} = e^* + \frac{1}{2}\kappa_\xi^2(\eta^2+\zeta^2), \quad \varepsilon_{22} = 0, \quad \varepsilon_{33} = 0$$
$$\varepsilon_{12} = \frac{1}{2}\kappa_\xi\left(\frac{\partial f}{\partial \eta} - \zeta\right), \quad \varepsilon_{13} = \frac{1}{2}\kappa_\xi\left(\frac{\partial f}{\partial \zeta} + \eta\right), \quad \varepsilon_{23} = 0 \tag{23}$$

To determine the strain energy, the following additional assumptions are stated:

{13} The material is isotropic.
{14} The material properties are homogeneous.
{15} The cross-section is symmetric about each of the $\mathbf{E}_1$–$\mathbf{E}_2$ and $\mathbf{E}_1$–$\mathbf{E}_3$ planes and does not vary along the length of the beam.

The initial tension T causes the beam to have uniaxial stress T/A in the reference configuration, where A is the cross-sectional area. When the beam experiences a strain ε_{11} away from χ^{r}, the initial tension causes a strain energy per unit volume of $(T/A)\varepsilon_{11}$. The strain energy per unit length is

$$U = \frac{1}{2}\int\int_A \left(2\frac{T}{A}\varepsilon_{11} + \sigma_{11}\varepsilon_{11} + \sigma_{22}\varepsilon_{22} + \sigma_{33}\varepsilon_{33} + \sigma_{12}\gamma_{12} + \sigma_{13}\gamma_{13} + \sigma_{23}\gamma_{23}\right) \mathrm{d}\eta\,\mathrm{d}\zeta \tag{24}$$

where σ_{ij} are stress increments of χ^{f} relative to χ^{r}, and γ_{ij} are engineering shear strain components that are related to the tensorial shear strain components by $\varepsilon_{ij} = \gamma_{ij}/2$. Using assumptions {7} and {13}, the constitutive equations are

$$\sigma_{11} = E\varepsilon_{11}, \quad \sigma_{12} = G\gamma_{12}, \quad \sigma_{13} = G\gamma_{13} \tag{25}$$

where E and G are Young's modulus and the shear modulus, respectively. Due to assumption {14} the mass centroid and area centroid of a cross-section coincide, giving

$$\int\int_A \eta\zeta\,\mathrm{d}\eta\,\mathrm{d}\zeta = \int\int_A \eta\,\mathrm{d}\eta\,\mathrm{d}\zeta = \int\int_A \zeta\,\mathrm{d}\eta\,\mathrm{d}\zeta = 0 \tag{26}$$

Insertion of (23), (25) and (26) into (24) gives

$$U = \frac{1}{8}\kappa_\xi^4 E\int\int_A (\eta^2+\zeta^2)^2\,\mathrm{d}\eta\,\mathrm{d}\zeta + \frac{1}{2}\kappa_\xi^2 E\int\int_A (\zeta\kappa_\eta - \eta\kappa_\zeta)(\eta^2+\zeta^2)\,\mathrm{d}\eta\,\mathrm{d}\zeta + \frac{1}{2}\kappa_\xi^2 D_\xi + \frac{1}{2}\kappa_\eta^2 D_\eta + \frac{1}{2}\kappa_\zeta^2 D_\zeta$$
$$+ \frac{1}{2}e_0^2 EA + \frac{1}{2}\kappa_\xi^2\left(e_0 + \frac{T}{EA}\right)(D_\eta + D_\zeta) + Te_0 \tag{27}$$

where cross-sectional area and the flexural rigidities are defined as

$$A = \int\int_A \mathrm{d}\eta\,\mathrm{d}\zeta, \quad D_\eta = E\int\int_A \zeta^2\,\mathrm{d}\eta\,\mathrm{d}\zeta, \quad D_\zeta = E\int\int_A \eta^2\,\mathrm{d}\eta\,\mathrm{d}\zeta \tag{28}$$

and where torsional rigidity is defined as (Love, 1944)

$$D_\xi = G\int\int_A \left[\left(\frac{\partial f}{\partial \zeta} + \eta\right)^2 + \left(\frac{\partial f}{\partial \eta} - \zeta\right)^2\right] \mathrm{d}\eta\,\mathrm{d}\zeta \tag{29}$$

Values of the integral in (29) are tabulated for various cross-sectional shapes (Timoshenko and Goodier, 1970). Due to assumption {15}, moments of area of order three are zero, and the second term on the right-hand side of (27) vanishes. The first term on the right-hand side of (27) contains a higher order moment of area and its contribution to the equations of motion is neglected. This is justified when the cross-sectional dimensions are small compared to the length. The assumption is

{16} moments of area of order four are neglected.

The final expression for strain energy per unit length is

$$U = \frac{1}{2}\left[\kappa_\xi^2 D_\xi + \kappa_\eta^2 D_\eta + \kappa_\zeta^2 D_\zeta + e_0^2 EA + \kappa_\xi^2\left(e_0 + \frac{T}{EA}\right)(D_\eta + D_\zeta) + 2Te_0\right] \tag{30}$$

where the κ_i are defined in (11).

2.3. Kinetic energy

The kinetic energy per unit length of a translating beam is given by

$$K = \frac{1}{2}\int\int_A \dot{\mathbf{r}}_\mathbf{P}^\mathrm{f} \cdot \dot{\mathbf{r}}_\mathbf{P}^\mathrm{f} \rho \,\mathrm{d}\eta\,\mathrm{d}\zeta \tag{31}$$

where ρ is density and $\mathbf{r}_\mathbf{P}^\mathrm{f}$ is defined in (16). Eq. (16) is decomposed as

$$\mathbf{r}_\mathbf{P}^\mathrm{f} = \mathbf{r}_\mathbf{E} + \mathbf{r}_\mathbf{e} \tag{32}$$

where $\mathbf{r}_\mathbf{E}$ and $\mathbf{r}_\mathbf{e}$ are the terms expressed in (16) on the $\mathbf{E}_i$ and $\mathbf{e}_i$ bases, respectively. It follows that

$$\dot{\mathbf{r}}_\mathbf{P}^\mathrm{f} \cdot \dot{\mathbf{r}}_\mathbf{P}^\mathrm{f} = \dot{\mathbf{r}}_\mathbf{E} \cdot \dot{\mathbf{r}}_\mathbf{E} + \dot{\mathbf{r}}_\mathbf{e} \cdot \dot{\mathbf{r}}_\mathbf{e} + 2\dot{\mathbf{r}}_\mathbf{E} \cdot \dot{\mathbf{r}}_\mathbf{e} \tag{33}$$

Recognizing that the material derivative introduces convective velocity terms, $\dot{\mathbf{r}}_\mathbf{E}$ is

$$\dot{\mathbf{r}}_\mathbf{E} = (\dot{u} + u'c + c)\mathbf{E_1} + (\dot{v} + v'c)\mathbf{E_2} + (\dot{w} + w'c)\mathbf{E_3} \tag{34}$$

Using assumption {7}, the terms $\dot{\eta}\mathbf{e_2}$ and $\dot{\zeta}\mathbf{e_3}$ are zero in the expression for $\dot{\mathbf{r}}_\mathbf{e}$. From assumption {11}, the contribution of cross-sectional warping to kinetic energy is neglected. With these assumptions and (4), the expression for $\dot{\mathbf{r}}_\mathbf{e}$ is

$$\dot{\mathbf{r}}_\mathbf{e} = (\omega_\eta\zeta - \omega_\zeta\eta)\mathbf{e_1} - \omega_\xi\zeta\mathbf{e_2} + \omega_\xi\eta\mathbf{e_3} \tag{35}$$

Using (34) and (35), when the term $2\dot{\mathbf{r}}_\mathbf{E} \cdot \dot{\mathbf{r}}_\mathbf{e}$ in (33) is integrated over the cross-section in (31) it vanishes due to (26). Using (31)–(35) and assumption {14}, the kinetic energy per unit length is

$$K = \frac{1}{2}\{m[(\dot{u} + u'c + c)^2 + (\dot{v} + v'c)^2 + (\dot{w} + w'c)^2] + j_\xi\omega_\xi^2 + j_\eta\omega_\eta^2 + j_\zeta\omega_\zeta^2\} \tag{36}$$

where m is the mass per unit length and the mass moments of inertia per unit length are defined as

$$j_\eta = \rho\int\int_A \zeta^2\,\mathrm{d}\eta\,\mathrm{d}\zeta, \quad j_\zeta = \rho\int\int_A \eta^2\,\mathrm{d}\eta\,\mathrm{d}\zeta, \quad j_\xi = j_\eta + j_\zeta \tag{37}$$

2.4. Nonlinear equations of motion

The variation of the specific Lagrangian $l = K - U$ is

$$\delta l = \sum_{i=1}^{15}\frac{\partial l}{\partial z_i}\delta z_i \tag{38}$$

where the z_i are components of

$$\mathbf{z} = \{\psi, \phi, \theta, \dot{u}, \dot{v}, \dot{w}, \dot{\psi}, \dot{\phi}, \dot{\theta}, u', v', w', \psi', \phi', \theta'\}^\mathrm{T} \tag{39}$$

The holonomic constraints in (1) yield

$$\delta\psi = \frac{\partial\psi}{\partial u'}\delta u' + \frac{\partial\psi}{\partial v'}\delta v', \quad \delta\phi = \frac{\partial\phi}{\partial u'}\delta u' + \frac{\partial\phi}{\partial v'}\delta v' + \frac{\partial\phi}{\partial w'}\delta w' \tag{40}$$

The system studied in this work is not subjected to any non-conservative forces, and the misalignment causing buckling occurs as an imposed inhomogeneous boundary condition at $x = L$; there is no virtual work

expression. Application of Hamilton's principle, $\int_{t_1}^{t_2}\int_0^L \delta l\,\mathrm{d}x\,\mathrm{d}t = 0$, yields the following equations of motion and boundary conditions:

$$G'_\alpha = \left(A_\psi \frac{\partial \psi}{\partial \alpha'} + A_\phi \frac{\partial \phi}{\partial \alpha'} - \frac{\partial l}{\partial \alpha'}\right)' = m(\ddot{\alpha} + c\dot{\alpha}') \quad \alpha = u, v, w \tag{41}$$

$$A_\theta = 0$$

$$A_\alpha = \frac{\partial^2 l}{\partial \dot{\alpha}\,\partial t} + \frac{\partial^2 l}{\partial \alpha'\,\partial x} - \frac{\partial l}{\partial \alpha}, \quad \alpha = \psi, \phi, \theta \tag{42}$$

$$\left(H_u \delta u' + H_v \delta v' + H_w \delta w' - G_u \delta u - G_v \delta v - G_w \delta w + \frac{\partial l}{\partial \theta'}\delta\theta\right)_{x=i} = 0, \quad i = 0, L \tag{43}$$

$$H_\alpha = \frac{\partial l}{\partial \psi'}\frac{\partial \psi}{\partial \alpha'} + \frac{\partial l}{\partial \phi'}\frac{\partial \phi}{\partial \alpha'}, \quad \alpha = u, v, w \tag{44}$$

When tension and translation speed are zero, (41)–(44) reduce to the equations in Crespo da Silva (1988) for a stationary, untensioned, flexural–flexural–torsional–extensional beam. (The equation for the Lagrange multiplier in Crespo da Silva (1988) has a typographical error that is addressed in a footnote in Crespo da Silva (1991).)

The non-dimensional variables used in this work are

$$\begin{aligned}
&\tilde{\alpha} = \frac{\alpha}{L} \ (\alpha = a, x, u, v, w), \quad \tilde{t} = t\sqrt{\frac{T}{mL^2}}, \quad \tilde{c} = c\sqrt{\frac{m}{T}} \\
&\beta_\xi = \frac{D_\xi}{TL^2}, \quad \beta_\eta = \frac{D_\zeta}{D_\eta}, \quad \beta_\zeta = \frac{D_\zeta}{TL^2}, \quad \mu = \frac{T}{EA} \\
&\tilde{j}_\alpha = \frac{j_\alpha}{mL^2}, \quad \tilde{\kappa}_\alpha = \kappa_\alpha L, \quad \tilde{\omega}_\alpha = \omega_\alpha\sqrt{\frac{mL^2}{T}} \ (\alpha = \xi, \eta, \zeta)
\end{aligned} \tag{45}$$

where a is the boundary misalignment along $\mathbf{E_3}$. The expressions for $\tilde{\kappa}_\alpha$ and $\tilde{\omega}_\alpha$ take the same form as (11) and (6) with the primes denoting the derivative with respect to $\tilde{x}$, the dots denoting the derivative with respect to $\tilde{t}$, and all c's replaced by $\tilde{c}$. The dimensionless specific Lagrangian is

$$\begin{aligned}
\tilde{l} &= \frac{l}{T} \\
&= \frac{1}{2}[(\dot{\tilde{u}} + \tilde{u}'\tilde{c} + \tilde{c})^2 + (\dot{\tilde{v}} + \tilde{v}'\tilde{c})^2 + (\dot{\tilde{w}} + \tilde{w}'\tilde{c})^2 + \tilde{j}_\xi\tilde{\omega}_\xi^2 + \tilde{j}_\eta\tilde{\omega}_\eta^2 + \tilde{j}_\zeta\tilde{\omega}_\zeta^2] \\
&\quad - \frac{1}{2}\left[\beta_\xi\tilde{\kappa}_\xi^2 + \frac{\beta_\zeta}{\beta_\eta}\tilde{\kappa}_\eta^2 + \beta_\zeta\tilde{\kappa}_\zeta^2 + \frac{1}{\mu}e_0^2 + \tilde{\kappa}_\xi^2(e_0 + \mu)\left(\frac{\beta_\zeta}{\beta_\eta} + \beta_\zeta\right) + 2e_0\right]
\end{aligned} \tag{46}$$

where again prime denotes the derivative with respect to $\tilde{x}$ and dot denotes the derivative with respect to $\tilde{t}$.

Hamilton's principle then takes the form $\int_{\tilde{t}_1}^{\tilde{t}_2}\int_0^1 \delta\tilde{l}\,\mathrm{d}\tilde{x}\,\mathrm{d}\tilde{t} = 0$. The non-dimensional equations of motion and boundary conditions are the same as in (41)–(44) except non-dimensional quantities are used and all derivatives are with respect to non-dimensional space and time.

2.5. Application to parallel pulley misalignment

For the remainder of this work, the three-dimensional translating beam theory developed in previous sections is applied to a continuum (belt, tape, band saw, etc.) undergoing parallel pulley misalignment. Under parallel pulley misalignment, the center of one pulley is displaced an amount a in the $\mathbf{E_3}$ direction.

Both span boundaries are modeled as clamped in the $\mathbf{E}_1$–$\mathbf{E}_2$ and $\mathbf{E}_1$–$\mathbf{E}_3$ planes. Assumptions {3} and {4} imply the beam adheres to the surface of the pulley beyond points G and H (Fig. 1). This is reasonable considering factors such as tension and frictional forces contribute to belt adhesion on the pulleys. Also, many belts have ribs that ride in grooves on the pulleys. At point G, for example, this provides a contact force against motion in the $\mathbf{E}_3$ direction and adds frictional forces against motion in the $\mathbf{E}_2$ direction. Because

the assumptions imply the belt adheres to the surface of the pulley directly beyond the span boundaries, the clamped boundary condition avoids a slope discontinuity at the boundaries.

The misalignment is modeled as an inhomogeneous boundary condition occurring at one end. The boundary conditions are

$$\begin{aligned} &\tilde{u}|_{x=i} = \tilde{v}|_{x=i} = \theta|_{x=i} = \tilde{v}'|_{x=i} = \tilde{w}'|_{x=i} = 0, \quad i = 0, 1 \\ &\tilde{w}|_{x=0} = 0, \quad \tilde{w}|_{x=1} = \tilde{a} \end{aligned} \tag{47}$$

2.6. Reduction of the equations of motion

The full nonlinear equations of motion given by (41) have structural features that make their solution difficult for the boundary conditions used in this work. In this section these difficulties are discussed and a reduction of the equations to a simpler form that avoids these issues is presented. Unless otherwise stated, nondimensional variables will be used and the tildes dropped for convenience.

When (41) are fully expanded the resulting equations contain four spatial derivatives of u, v, and w and three spatial derivatives of θ. The boundary conjunct (43), however, yields only one boundary condition at each of $x = 0$, 1 for θ. Only two boundary conditions are apparent for a third order boundary value problem for θ. In addition, H_u in (43) vanishes for clamped–clamped boundary conditions. In other words, the natural boundary conditions associated with u' at $x = 0$, 1 are automatically satisfied for clamped–clamped boundaries. The cause of this can be noted in (44) where the term $\partial\psi/\partial u' = 0$ when $v' = 0$ and the term $\partial\phi/\partial u' = 0$ when $w' = 0$. Therefore, when (41) are fully expanded in terms of u, v, w, and θ, boundary conditions appear to be missing. While Hamilton's principle will generate a well-posed problem with sufficient equations and boundary conditions to obtain a solution, these occur here in an imbalanced form where there are three fewer boundary conditions than total order of the spatial derivatives in the governing equations. This complicates any numerical or analytical solution. In a simpler system, mathematical manipulations would likely allow reformulation in a balanced form, but the length of the present equations precludes this. This issue is resolved, however, by a physically justifiable assumption that is later verified.

All terms containing θ''' originate from higher order terms in κ_ξ and ω_ξ. κ_ξ in (11) contains two distinct components, namely, the cross-sectional twist, θ', and the geometric torsion, $\psi' \sin\phi$. The cross-sectional twist results from the final Euler angle rotation of the cross-section about the $\mathbf{e_1}$ axis. The geometric torsion arises from centerline displacements regardless of cross-sectional considerations and is non-zero only when the centerline has both curvature in the $\mathbf{e_1} - \mathbf{e_3}$ ($\mathbf{e_1} - \mathbf{e}_2$) plane and non-zero displacement in the $\mathbf{e_2}$ ($\mathbf{e_3}$) direction. The expression for ω_ξ contains analogous components. The terms containing θ''' originate from the geometric torsion components of κ_ξ and ω_ξ.

When a clamped–clamped beam undergoes transverse displacement, midplane stretching is important, so the inextensibility assumption was not used. The axial stiffness of a belt, band saw, tape drive, or the like is typically much higher than the flexural and torsional stiffnesses. Due to this property, when a clamped–clamped beam experiences transverse displacement, midplane stretching is resisted by the relatively high axial stiffness. From (3), axial strain is not a function of θ, so a high axial stiffness does not resist twist. For this reason, when the beam buckles out-of-plane as in the problem of interest, one expects the twist to be much larger than the geometric torsion. Therefore, the following assumption is made:

{17} The geometric torsion components of κ_ξ and ω_ξ are neglected.

Under this assumption

$$\begin{aligned} \kappa_\xi &= \theta' \\ \omega_\xi &= \dot{\theta} + \theta' c \end{aligned} \tag{48}$$

In general, θ is not a true twisting angle, as stated in Pai and Nayfeh (1990): "It can be shown that any twist variable [θ], defined using a sequence of three Euler-like rotations or even two sequential rotations, is not a real twisting angle because the deformations u, v, w, and [θ] do not occur in sequence as assumed in

the mathematical model that uses Euler angles." A true cross-sectional twist angle, γ, can be defined by $\kappa_\xi = \gamma'$. As a consequence of assumption {17} θ becomes a true twist angle.

For assumption {17} to be appropriate the geometric torsion must be small and small compared to the twist. The geometric torsion is a function of the derivatives of u, v, and w. Therefore, u, v, w, and their derivatives are ordered as small quantities using the expansion parameter ε where $\varepsilon \ll 1$ is a small parameter of magnitude $\varepsilon = O(\sqrt{\mu})$. Under this definition, the strain $\mu = T/EA$ that brings the system from the undeformed configuration into the tensioned reference configuration is $O(\varepsilon^2)$. Due to the boundary conditions (47), longitudinal displacement occurs only as a result of axial strain arising from transverse displacement. Thus, it is reasonable to order u and its derivatives as $O(\varepsilon^2)$, while v, w, and their derivatives are $O(\varepsilon)$. θ and its derivatives are specified as being O(1).

Taylor series expansion of the equations of motion, including the reduced expressions in (48), is performed through order ε^2. The reduced equations of motion and boundary conditions are

$$\begin{aligned} &\widehat{G}'_\alpha = \ddot{\alpha} + \dot{\alpha}' c, \quad \alpha = u, v, w \\ &\widehat{G}_\theta = 0 \end{aligned} \tag{49}$$

$$(\widehat{H}_u \delta u' + \widehat{H}_v \delta v' + \widehat{H}_w \delta w' - \widehat{G}_u \delta u - \widehat{G}_v \delta v - \widehat{G}_w \delta w + \widehat{H}_\theta \delta\theta)_{x=i} = 0, \quad i = 0, 1 \tag{50}$$

where expressions for the $\widehat{G}_\alpha$ and $\widehat{H}_\alpha$ are given in Appendix A. As a result of this reduction u''' and u^{IV} (fourth spatial derivative) terms are removed. In addition, by invoking assumption {17} the highest spatial derivative of θ is now two. Like H_u in (43), $\widehat{H}_u$ in (50) also vanishes for clamped–clamped boundary conditions. Consequently, for a clamped–clamped beam the equations of motion are reduced to a balanced form in which the number of boundary conditions matches the number of spatial derivatives.

The equations of motion reduce to the well-known equations for flexural–extensional motion of a translating, tensioned beam (Mote and Wu, 1985; Wang and Mote, 1986; Wickert, 1992). To reduce (49) to the flexural–extensional model, θ, w, and mass moments of inertia are set to zero. The resulting equations are cast in dimensional form for comparison, giving

$$m\ddot{u} + 2mc\dot{u}' + mc^2 u'' - EAv'v'' - EAu'' - D_\zeta v' v^{IV} - D_\zeta v'' v''' + 2EAv'v''u' + EAv'^2 u'' + \frac{3}{2}EAv'^3 v'' + Tv'v'' = 0 \tag{51}$$

$$m\ddot{v} + 2mc\dot{v}' + mc^2 v'' - EAu'v'' - EAu''v' - \frac{3}{2}EAv'^2 v'' - Tv'' + D_\zeta v^{IV} = 0 \tag{52}$$

Eqs. (51) and (52) match the corresponding equations in Mote and Wu (1985), Wang and Mote (1986) and Wickert (1992) with the exception that (51) contains the additional terms $(EAv'^2u')' + \frac{3}{2}EAv'^3v'' + Tv'v'' - (D_\zeta v'v''')'$. The term $-(D_\zeta v'v''')'$ originates from higher order terms in κ_ζ included in the present work. The other additional terms originate from higher order terms in the axial strain. To get exact agreement with the previously published model e_0 in (3) and κ_ζ in (11) must be reduced to

$$\begin{aligned} e_0 &= u' + \frac{1}{2}v'^2 \\ \kappa_\zeta &= v'' \end{aligned} \tag{53}$$

3. Equilibrium analysis

The equations governing steady motions (referred to herein as equilibria) are obtained by setting all time derivatives to zero in (49). The boundary conditions are given in (47). The deformation results from boundary displacement in the $\mathbf{E_3}$ direction, $w|_{x=1} = a$ in dimensionless form.

Because the equilibrium equations are linear in the highest spatial derivatives, the boundary value problem can be expressed in the first order form

$$\mathbf{y}' = f(\mathbf{y}) \tag{54}$$

$$\mathbf{y} = \{u, u', v, v', v'', v''', w, w', w'', w''', \theta, \theta'\}^{\mathrm{T}} \tag{55}$$

The equilibrium equations are solved using continuation and bifurcation software (Doedel et al., 1997). With the trivial equilibrium as the initial solution and the boundary misalignment as the continuation parameter, the evolving equilibrium solution is followed as the misalignment changes. The critical buckling misalignments at which non-planar equilibria bifurcate from the planar equilibrium are detected. By switching branches at the bifurcation point, the bifurcated branch is followed and the non-planar post-buckled shape is determined for increasing misalignment. The stability of the branches is simply given in this paper with a more detailed discussion of its determination given in Part II of this work (Orloske and Parker, this issue).

The baseline numerical values of the system parameters are given in Table 1. Unless otherwise stated, these parameter values are used.

3.1. Planar equilibrium solutions

When continuation is performed in the misalignment parameter a, one equilibrium solution of the beam remains planar ($v = \theta = 0$) with no cross-sectional twist or transverse deflection in the $\mathbf{E_2}$ direction. The effect of translation speed on the planar equilibrium is assessed by using the translation speed c as the continuation

Table 1
Baseline values of system parameters

Dimensionless variable	Baseline value
$\tilde{c}$	0.3
β_ξ	0.002
β_η	0.001
β_ζ	0.0015
$\tilde{j}_\xi$	0.0019
$\tilde{j}_\eta$	0.0019
$\tilde{j}_\zeta$	0.000019
μ	0.0029

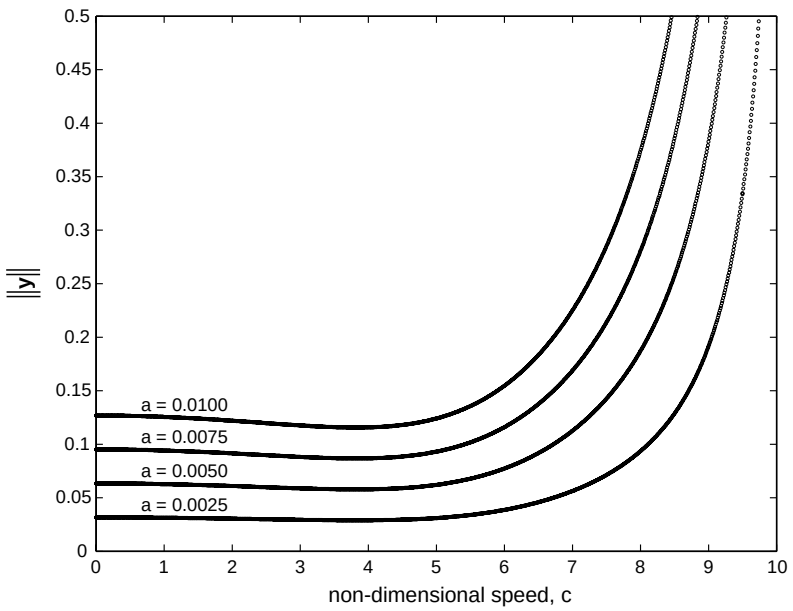

Fig. 5. The L_2-norm of planar equilibrium solutions for different misalignments.

parameter. Fig. 5 illustrates this effect for four different misalignments. The L_2-norm of the state vector $\mathbf{y}$ in (55) is defined by

$$\|\mathbf{y}\| = \sqrt{\int_0^1 \sum_{i=1}^{12} y_i^2 \, \mathrm{d}x} \tag{56}$$

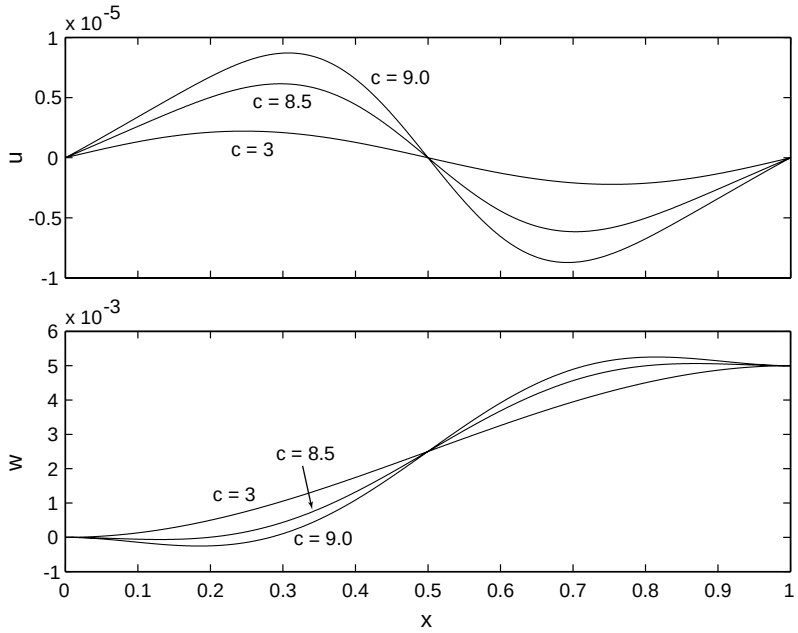

Fig. 6. Selected planar equilibrium solutions for $a = 0.005$.

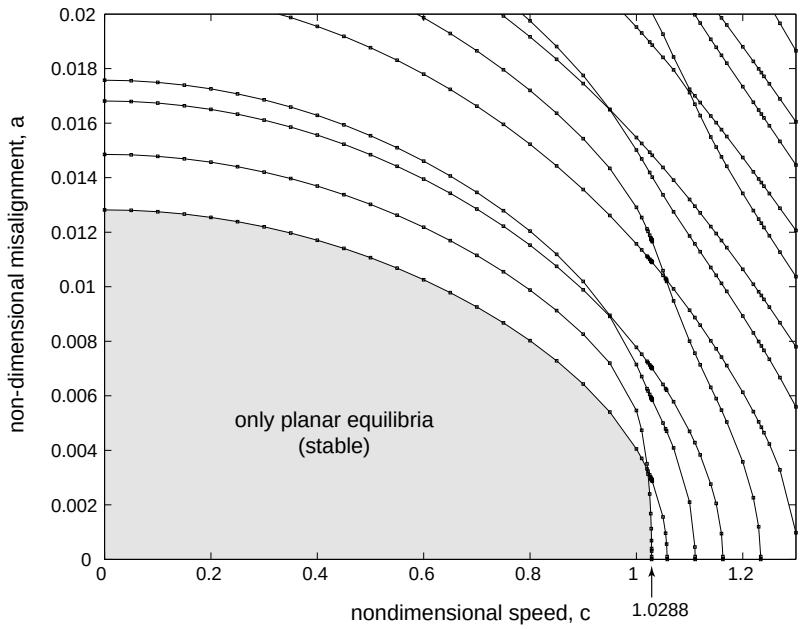

Fig. 7. Critical misalignments and speeds where non-planar equilibria bifurcate from the planar equilibrium.

where the y_i are components of $\mathbf{y}$. In Fig. 5 the planar solutions for the selected misalignments undergo little change for speeds up to approximately $c = 5$. When the speed is increased further the solutions change rapidly. As misalignment is increased, this region of rapid change occurs at lower speeds. This implies that the

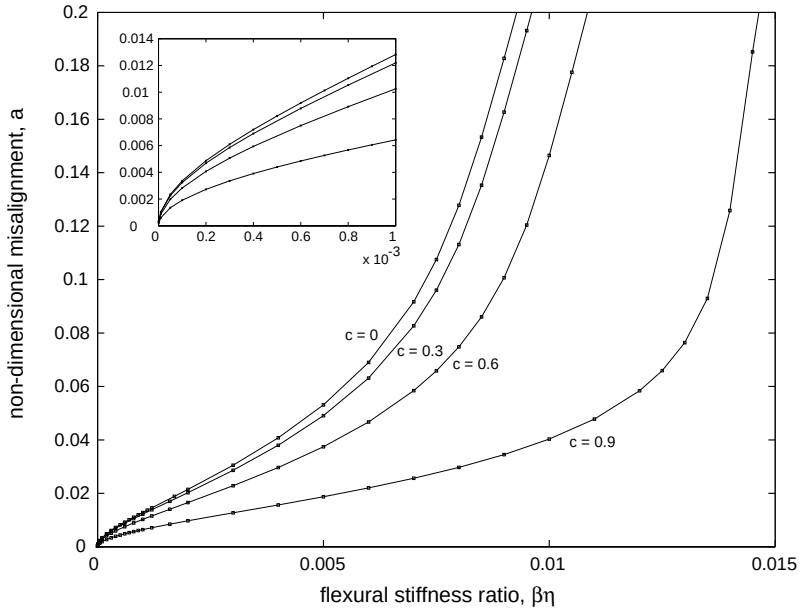

Fig. 8. Influence of the flexural stiffness ratio on the lowest critical misalignment.

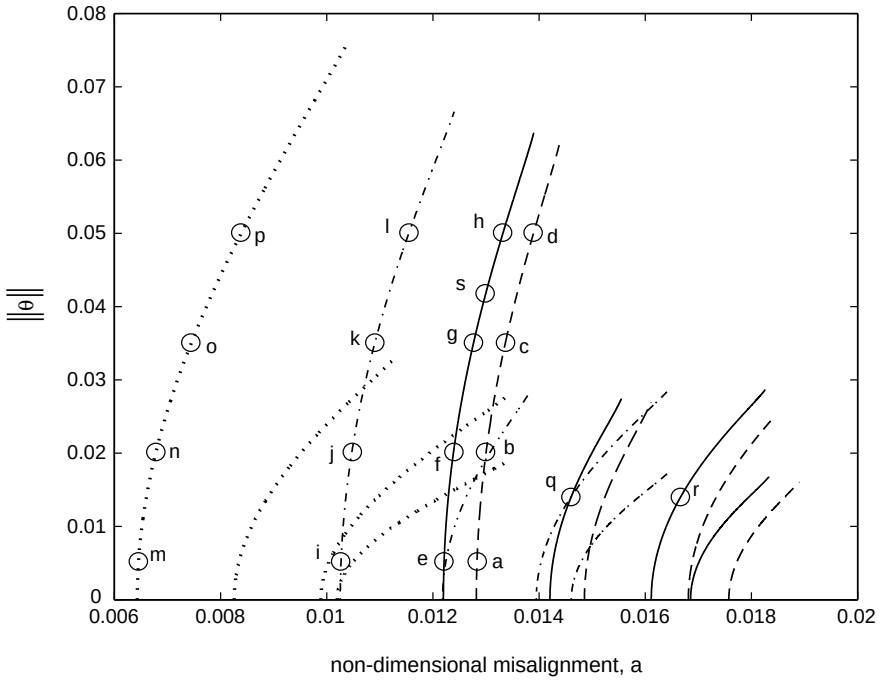

Fig. 9. The first four bifurcation branches for four different translation speeds. The dashed curves represent $c = 0$, the solid curves $c = 0.3$, the dash dot curves $c = 0.6$, and the dotted curves $c = 0.9$. Point s is at the same misalignment as point b. Points e and q lie on the solid curves and point b lies on the dashed curve. The planar solution lies along the abscissa.

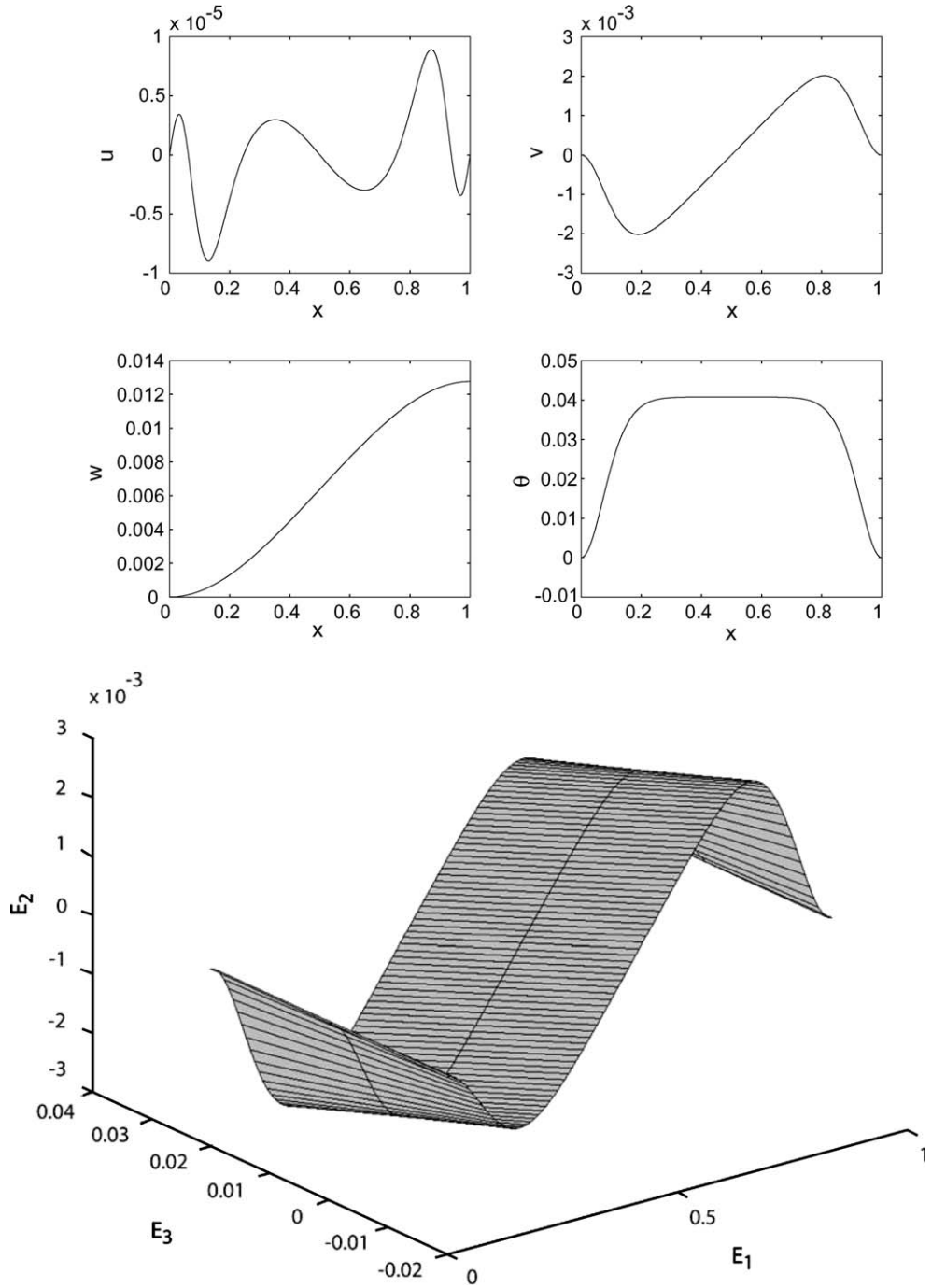

Fig. 10. The solution at point g in Fig. 9. In the three-dimensional plot, the width of the beam is set to 0.04 to show cross-sectional rotation.

influence of translation speed on the planar equilibrium solution occurs at lower speeds as the misalignment is increased.

Fig. 6 shows three solutions for a misalignment of $a = 0.005$ and illustrates how the planar equilibrium changes as speed is increased. As the translation speed increases, the shapes of the u and w solutions change and the magnitude of the u solution increases rapidly, although it remains small compared to w.

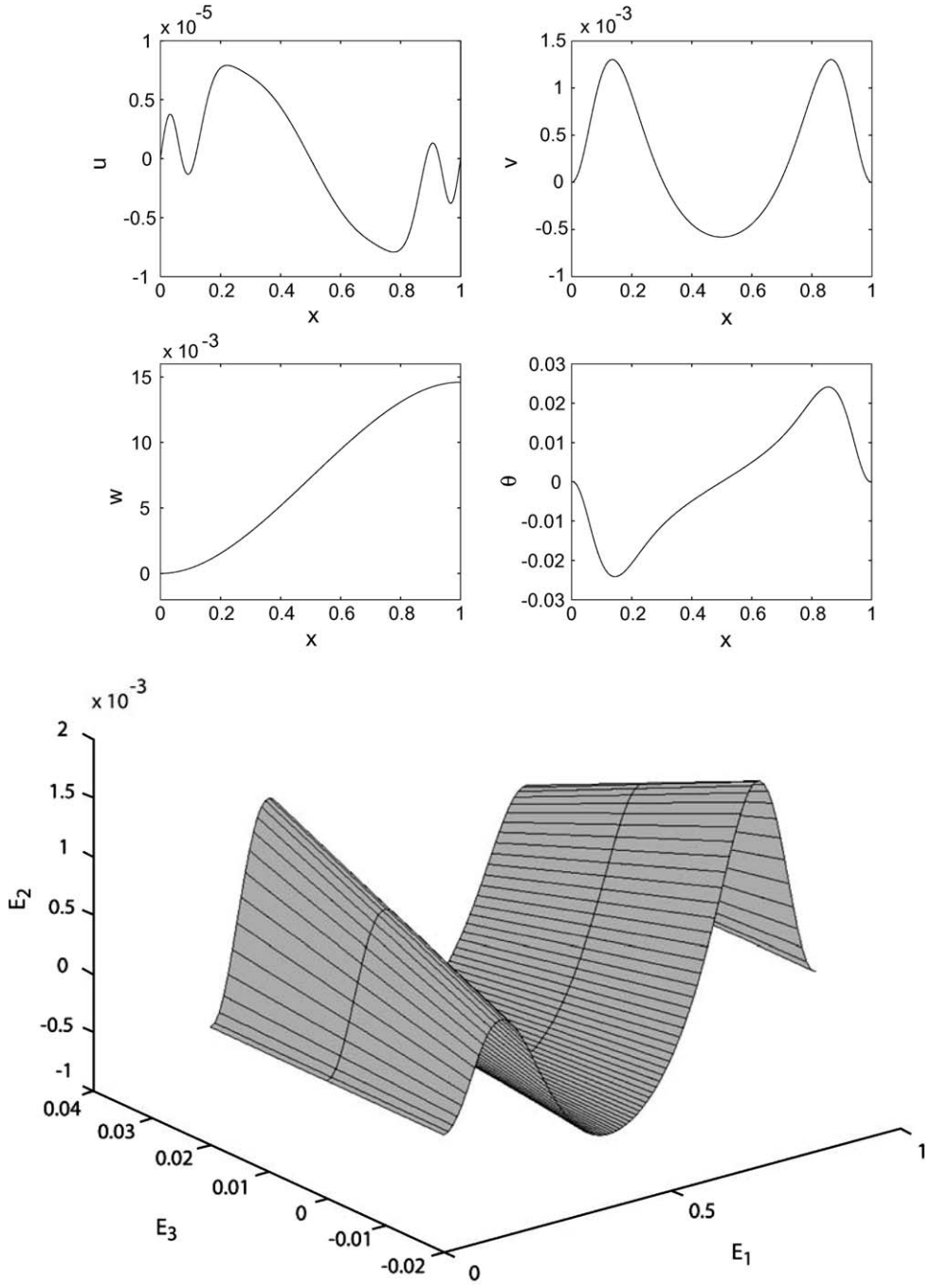

Fig. 11. The solution at point q in Fig. 9. In the three-dimensional plot, the width of the beam is set to 0.04 to show cross-sectional rotation.

The critical buckling misalignments occur when new equilibria bifurcate from the planar solution. The bifurcated equilibria are non-planar. Fig. 7 displays these critical misalignments for translation speeds of $0 \leqslant c \leqslant 1.3$. The critical misalignments all decrease monotonically with increasing speed. The rate of decrease accelerates at higher speeds, indicating that the effect of speed on the critical misalignment is more pronounced as speed increases. In addition, the critical misalignments approach zero for large speeds. The speeds at which

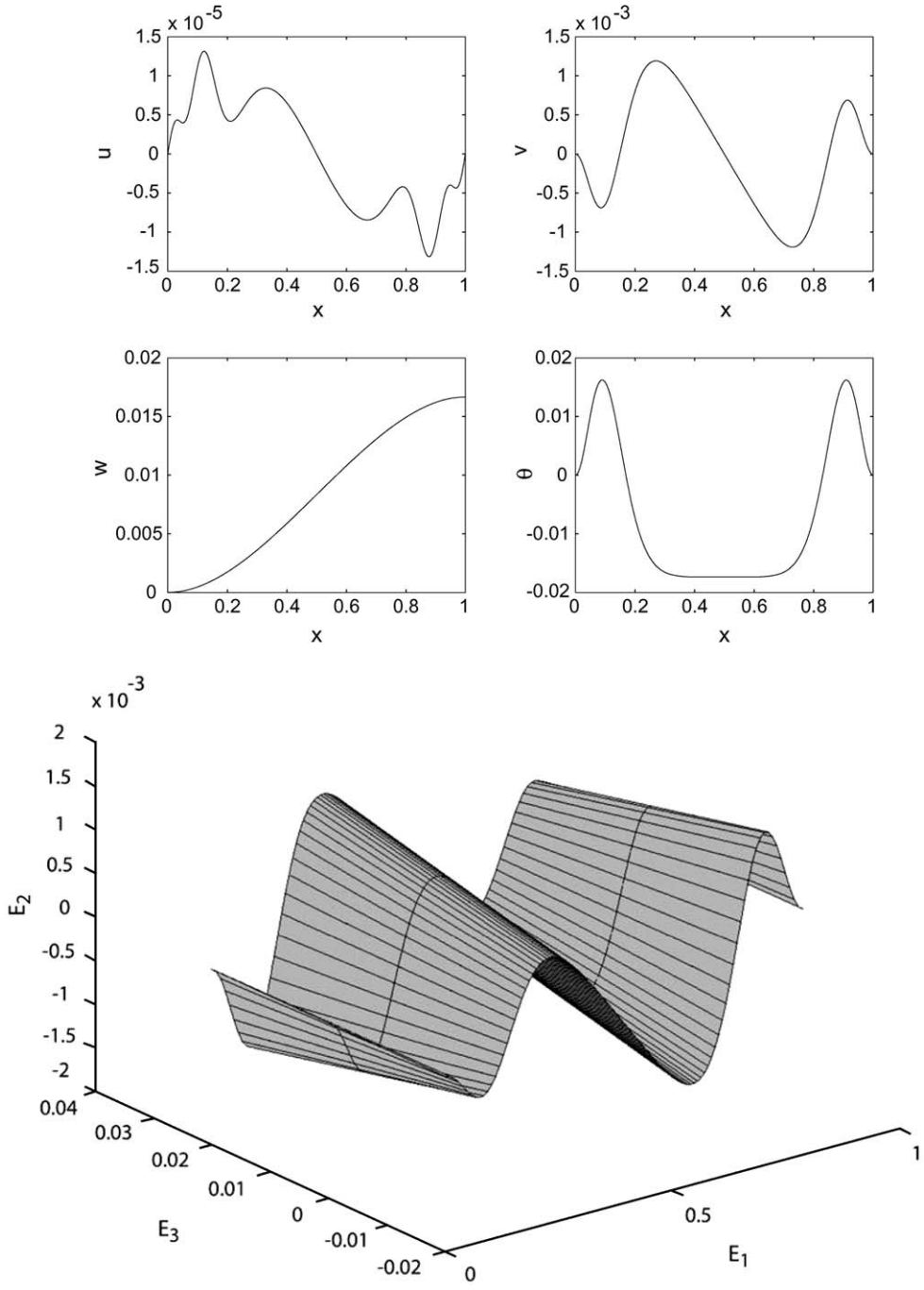

Fig. 12. The solution at point r in Fig. 9. In the three-dimensional plot, the width of the beam is set to 0.04 to show cross-sectional rotation.

the critical misalignment loci touch the abscissa in Fig. 7 are the critical speeds for zero misalignment. As will be discussed in Part II (Orloske and Parker, this issue), these zero misalignment critical speeds are the same as the well-known critical speeds common in the axially moving materials literature, that is, the speeds at which an eigenvalue of the dynamic equations linearized about the trivial solution vanishes. The first zero misalignment critical speed corresponds to the speed at which the trivial equilibrium becomes unstable and occurs at

$c = 1.0288$. For speeds less than $c = 1.0288$, planar equilibrium stability is lost at the first branch point for increasing misalignment. For example, at a speed of $c = 0.3$ the critical misalignment is $a = 0.0122$. The region in the lower left of Fig. 7 indicates the region where the planar equilibrium is the only one, and it is stable.

The critical misalignment loci in Fig. 7 consistently cross in pairs of two. This causes the post-buckled shapes to change the order in which they occur. For example, when the misalignment $a = 0.004$ is specified and speed is increased, the first two detected critical speeds correspond to particular post-buckled shapes. If instead the misalignment is $a = 0.002$ and speed is increased, the occurrence of the post-buckled shapes exchanges order.

In addition to speed, the flexural stiffness ratio β_η (see (45)) greatly influences the critical misalignment. One expects that as the beam becomes more compliant in the $\mathbf{e_1}$–$\mathbf{e_2}$ plane (i.e., small β_η), the critical misalignment decreases. This expectation is supported in Fig. 8, which demonstrates that as the ratio of flexural stiffnesses approaches zero, the lowest critical misalignment approaches zero in a manner asymptotic to the vertical axis (inset of Fig. 8). The shape of the loci for $\beta_\eta \approx 0$ shows that even for infinitesimal β_η, a finite misalignment is required to buckle the beam for any speed. For higher flexural stiffness ratios the curvature of the plot changes, eventually reaching a point of high slope that suggests each speed has, at least in practical terms, a maximum stiffness ratio above which no flexural–torsional buckling occurs. For all flexural stiffness ratios, translation speed decreases the critical misalignments, and its impact increases with increasing speed. This is illustrated by observing that the difference between two adjacent curves increases as speed increases.

3.2. Out-of-plane equilibria

When continuation is performed in misalignment, the planar equilibrium solution experiences pitchfork bifurcations at the critical misalignments. The two bifurcated equilibria are out-of-plane solutions. The L_2-norms of the individual deformation components of $\mathbf{y}$ in (55), $\|y_i\| = (\int_0^1 y_i^2 \, dx)^{1/2}$, are used to describe the out-of-plane solutions.

The first four bifurcation branches for translation speeds of $c = 0$, 0.3, 0.6, and 0.9 are shown in Fig. 9. The symmetry of the system about the $\mathbf{E}_1$–$\mathbf{E}_3$ plane is reflected in the symmetry of the pitchfork bifurcation

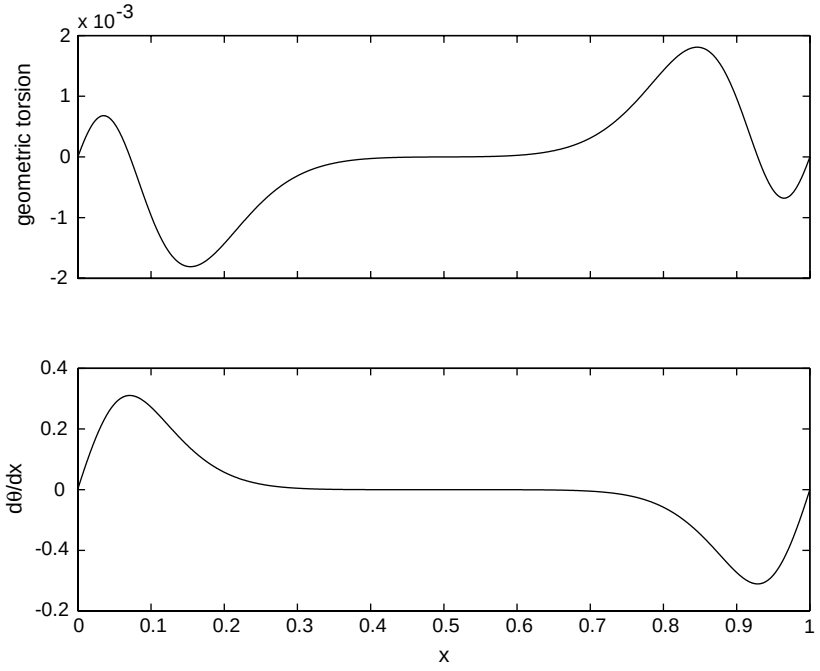

Fig. 13. Plot of the components of κ_ξ for the solution at point g in Fig. 9.

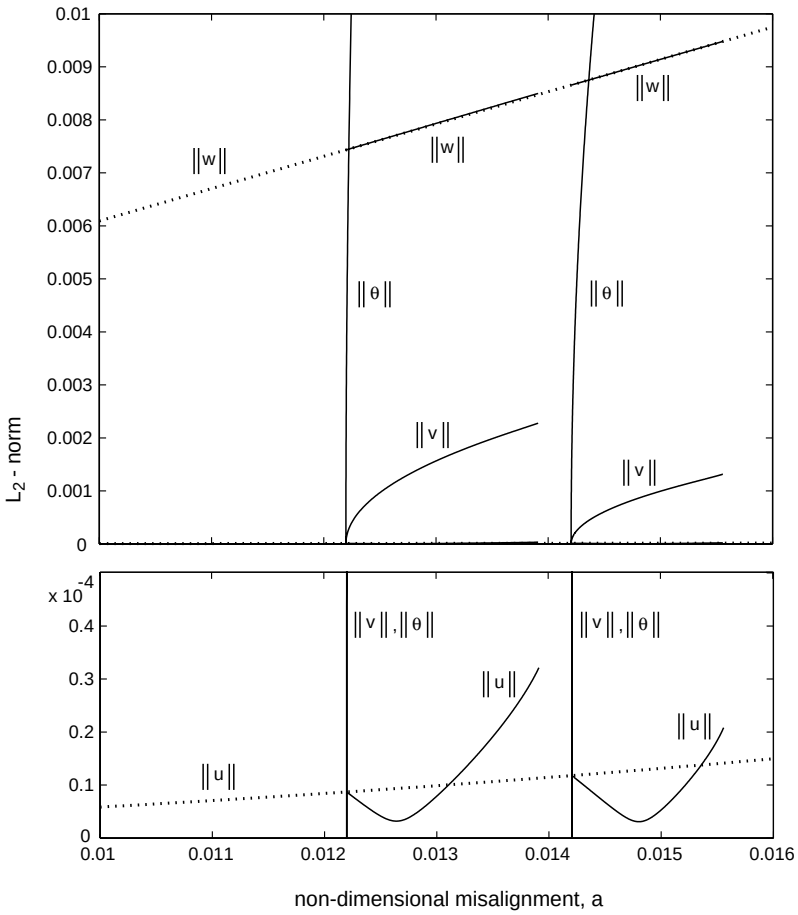

Fig. 14. L_2-norms of the deformation components for the first two bifurcation branches for varying misalignment when $c = 0.3$. $\|u\|$ is shown at the bottom on an expanded scale. The dotted line corresponds to the planar solution.

branches. The solution along one branch is identical to the solution along the other branch except the out-of-plane solution components v and θ are reflected such that $\alpha(x)$ becomes $-\alpha(x)$ where $\alpha = v, \theta$. With the measure $\|\theta\|$ the two out-of-plane branches of the pitchfork bifurcation lie on top of one another.

To obtain the form (54), the equilibrium equations are solved for the highest derivative terms. The resulting four equations for u'', v^{IV}, w^{IV}, and θ'' involve quotients. For certain out-of-plane solutions, the denominator of one of these quotients approaches zero. These singularities cause loss of convergence during continuation along the bifurcated branches. This limits the distance one can travel along the out-of-plane solution branches using continuation. The singularities occur where the branches stop in Fig. 9.

Solutions on the first three branches for the baseline translation speed $c = 0.3$ are plotted in Figs. 10–12. For speeds up to approximately $c = 0.9$ these post-buckled shapes change only slightly for the range of misalignments explored. This is reflected in Fig. 9 where for speeds of $c = 0$, 0.3, and 0.6 all four branches have almost identical shapes. Generally, the v and θ components of the out-of-plane solutions exhibit sharp change near the boundaries due to the clamped–clamped boundary conditions. Beam stresses will be highest near the boundaries during flexural–torsional buckling. This sharp change causes the higher derivatives of v to no longer be small near the boundaries. Recall that in the ordering scheme used to simplify the equations of motion, v and its derivatives are assumed to be small, so the validity of the ordering scheme breaks down near the boundaries for solutions further out on the branches. This may relate to the singularities noted above, in which case, including higher order terms would enable further travel on the branches.

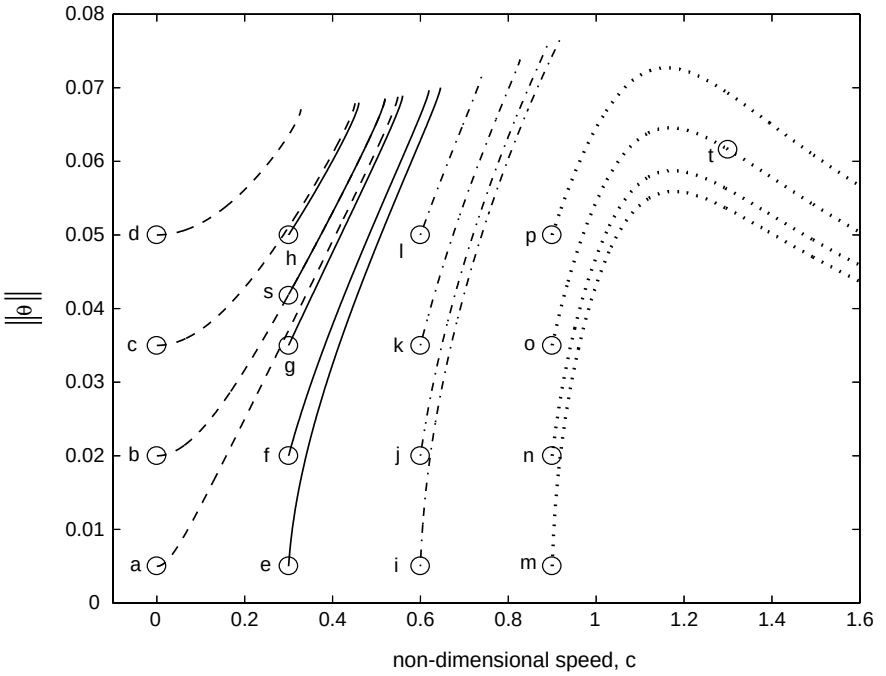

Fig. 15. Bifurcation branches obtained by performing continuation in speed from the labeled points in Fig. 9. Point t is at $c = 1.3$.

To check whether assumption {17} holds along the branches, the geometric torsion is compared to θ'. Fig. 13 shows an example of this comparison for the solution in Fig. 10. Note that the geometric torsion is two orders of magnitude lower than θ'. This result is typical for the out-of-plane solutions encountered in this work.

The values of $\|\alpha\|$, where $\alpha = u, v, w, \theta$, show how the deformation is distributed among the various degrees of freedom. Fig. 14 illustrates this comparison for the first two bifurcation branches with $c = 0.3$. Although the first two post-buckled shapes look very different (Figs. 10 and 11), Fig. 14 indicates the various L_2-norms are similar for the two branches, which suggests the deformation is distributed among the degrees of freedom in a similar manner. The variation in $\|w\|$ from the planar solution is extremely small indicating the w component of the out-of-plane solution undergoes very little change when moving from a planar solution to an out-of-plane one. This is consistent with the solutions in Figs. 10–12. In contrast, $\|u\|$ varies from the planar solution by first decreasing and then, for greater misalignments, increasing above that of the planar solution. For the distance traveled on the bifurcation branches, the magnitude of $\|v\|$ is always much greater than the change in $\|w\|$ compared to the planar solution (solid versus dashed lines). This is due to small β_η. At buckling, nearly all additional bending deflection is in the compliant $\mathbf{E_2}$ (v) direction; there is virtually no change in w relative to the planar solution as a result of buckling.

Fig. 15 explores the effect of buckling the beam into the first out-of-plane equilibrium by increasing misalignment past the critical value for a given speed and then increasing translation speed for fixed misalignment. The labeled points in this figure correspond to the labeled points in Fig. 9. Points at the top of the plot where the solution branches end are due to singularities that prevent further continuation. For speeds less than approximately $c = 0.9$, the shapes of the equilibrium solutions remain fairly unchanged as speed is increased. For higher speeds, the post-buckled shape changes, and this is reflected in the curves changing shape at the right of Fig. 15. The equilibrium solution at point t from this region is given in Fig. 16. In contrast to the lower speed regime, the post-buckled shape at point t in Fig. 15 experiences a less localized change at the boundaries and a greater share of transverse deflection v compared to cross-sectional twist θ. This trend may possibly occur at lower speeds and higher misalignments (for example branches i, j, k, l in Fig. 15) but the singularities prevent exploring this.

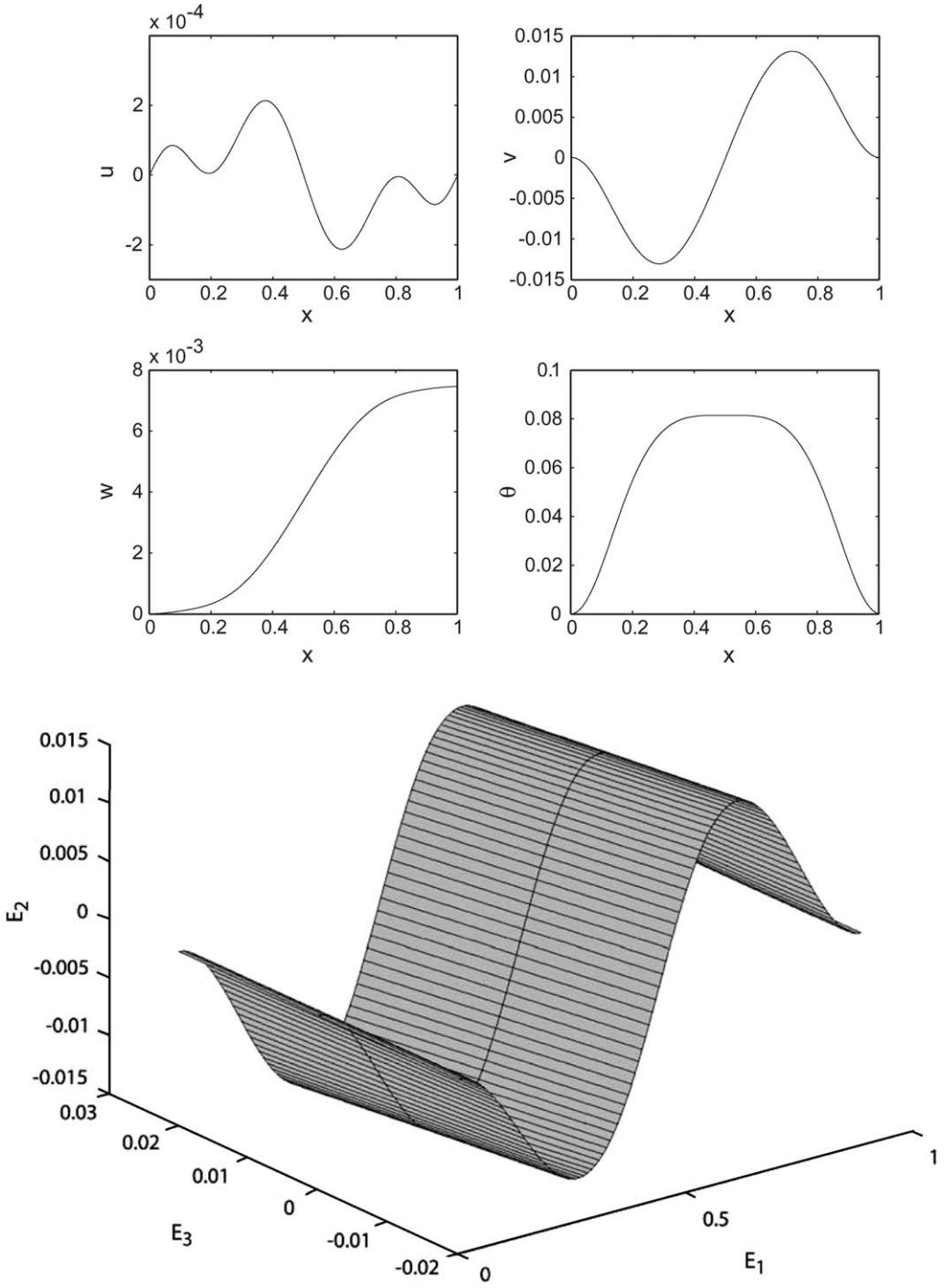

Fig. 16. The solution at point t in Fig. 15. In the three-dimensional plot, the width of the beam is set to 0.04 to show cross-sectional rotation.

The post-buckled shapes may be arrived at through different sequences of misalignment and speed. For example, the solution at point s in Fig. 9 can be reached by setting $c = 0.3$ and then increasing misalignment such that one travels along the first out-of-plane solution branch in Fig. 9. Alternatively, the same solution can be obtained by first setting $c = 0$ and then increasing misalignment such that one travels along the branch in

Fig. 9 to point b. Then, by increasing speed from point b, Fig. 15 illustrates that point s is reached when $c = 0.3$.

4. Conclusions

A nonlinear model is formulated to describe the motion of a translating, tensioned beam in three-dimensional space. The model accounts for geometric and inertia nonlinearities arising from flexure in two planes, torsion, and extension. The equations of motion indicate:

- Under the pulley misalignment boundary conditions of interest, the full nonlinear equations of motion occur in an unbalanced (although well-posed) form with fewer boundary conditions than total order of spatial derivatives. This form precludes use of standard numerical techniques. By neglecting geometric torsion and using a physically appropriate ordering scheme, the equations of motion reduce to a balanced form in which the number of boundary conditions matches the number of spatial derivatives.
- Under appropriate simplifying assumptions, the equations of motion reduce to equations in the literature for flexural–extensional motion of a translating, tensioned beam.

Continuation and bifurcation software is used to obtain equilibrium solutions for ranges of speed, misalignment, and flexural stiffness ratio. The equilibrium solutions indicate:

- When pulley misalignment occurs at speeds where the trivial equilibrium is stable, the initial equilibria are planar with no cross-sectional twist or out-of-plane transverse deflection. The critical misalignments at which new equilibria bifurcate from the planar equilibria decrease monotonically with increasing translation speed. The impact of speed on the critical misalignments is more pronounced as speed increases.
- The first critical misalignment is strongly influenced by the flexural stiffnesses ratio, β_η. For infinitesimal β_η a finite misalignment is required to buckle the beam for any speed, while at high β_η the results suggest there is a maximum stiffness ratio above which no flexural–torsional buckling occurs. For the entire range of β_η considered, the first critical misalignment remains strongly influenced by translation speed, and this influence is more pronounced as speed increases.
- At each critical misalignment a pitchfork bifurcation occurs. The pitchfork branches represent out-of-plane post-buckled configurations. Out-of-plane buckling deformation is predominantly transverse deflection in the compliant plane and cross-sectional twist. The solutions indicate sharp curvature and hence high stresses near the boundaries. Out-of-plane equilibria display small geometric torsion relative to cross-sectional twist, consistent with the assumptions, and minimal change in in-plane transverse deflection compared to the planar solutions.

Appendix A

The expressions for the $\widehat{G}_\alpha$ in (49) are

$$\begin{aligned}\widehat{G}_\alpha &= \Lambda_{\alpha 1}\cos^2\theta + \Lambda_{\alpha 2}\sin\theta\cos\theta + \Lambda_{\alpha 3}\sin^2\theta + \Lambda_{\alpha 4}\frac{1}{2\mu} + \Lambda_{\alpha 5}\frac{\beta_\zeta}{\beta_\eta}, \quad \alpha = u, v, w \\ \widehat{G}_\theta &= \Lambda_{\theta 1}\cos^2\theta + \Lambda_{\theta 2}\cos\theta\sin\theta + \Lambda_{\theta 3}\sin^2\theta + \Lambda_{\theta 4} + \Lambda_{\theta 5}\frac{\beta_\zeta}{\beta_\eta}\end{aligned} \tag{A.1}$$

where the $\Lambda_{\alpha i}$ are

$$\begin{aligned}\Lambda_{u1} = &-\{[w'\theta'v'' + v'(v''' + w''\theta')]c^2 + [w'(v''\dot\theta + \dot v'\theta') + v'(\dot w'\theta' + 2\dot v'' + w''\dot\theta)]c + w'\dot\theta\dot v' \\ &+ v'(\ddot v' + \dot w'\dot\theta)\}j_\zeta - \{[w'(w''' - \theta'v'') - v'\theta'w''']c^2 + [w'(-\dot v'\theta' + 2\dot w'' - v''\dot\theta) - v'(w''\dot\theta + \dot w'\theta')]c \\ &+ w'(\ddot w' - \dot v'\dot\theta) - v'\dot\theta\dot w'\}j_\eta + [w'\theta'v'' + v'(v''' + w''\theta')]\beta_\zeta\end{aligned} \tag{A.2}$$

$$\begin{aligned}\Lambda_{u2} &= \{[w'(-v''' - 2w''\theta') - v'(w''' - 2\theta' v'')]c^2 + [2w'(-\dot{w}'\theta' - \dot{v}'' - w''\dot{\theta}) + 2v'(v''\dot{\theta} - \dot{w}'' + \dot{v}'\theta')]c \\ &\quad - w'(2\dot{w}'\dot{\theta} + \ddot{v}') + v'(2\dot{v}'\dot{\theta} - \ddot{w}')\}j_\zeta + \{[w'(v''' + 2w''\theta')v'(w''' - 2\theta' v'')]c^2 \\ &\quad + [2w'(\dot{w}'\theta' + \dot{v}'' + w''\dot{\theta}) - 2v'(v''\dot{\theta} - \dot{w}'' + \dot{v}'\theta')]c + w'(2\dot{w}'\dot{\theta} + \ddot{v}') - v'(2\dot{v}'\dot{\theta} - \ddot{w}')\}j_\eta \\ &\quad + [w'(v''' + 2w''\theta') + v'(w''' - 2\theta' v'')]\beta_\zeta \end{aligned} \tag{A.3}$$

$$\begin{aligned}\Lambda_{u3} &= -\{[w'(w''' - \theta' v'') - v'\theta' w'']c^2 + [w'(-\dot{v}'\theta' + 2\dot{w}'' - v''\dot{\theta}) - v'(w''\dot{\theta} + \dot{w}'\theta')]c + w'(\ddot{w}' - \dot{v}'\dot{\theta}) \\ &\quad - v'\dot{\theta}\dot{w}'\}j_\zeta - \{[w'\theta' v'' + v'(v''' + w''\theta')]c^2 + [w'(v''\dot{\theta} + \dot{v}'\theta') + v'(\dot{w}'\theta' + 2\dot{v}'' + w''\dot{\theta})]c + w'\dot{\theta}\dot{v}' \\ &\quad + v'(\ddot{v}' + \dot{w}'\dot{\theta})\}j_\eta + [w'(w''' - \theta' v'') - v'\theta' w'']\beta_\zeta \end{aligned} \tag{A.4}$$

$$\begin{aligned}\Lambda_{u4} &= -\frac{1}{2}\theta'^2(-2 + w'^2 + v'^2)\mu\beta_\zeta + [(-2u' - 2)c^2 - 2\dot{u}c - v'^2 - w'^2 + 2]\mu - \frac{3}{4}w'^4 - \frac{3}{4}v'^4 \\ &\quad + w'^2\left(1 - 2u' - \frac{3}{2}v'^2\right) + v'^2(1 - 2u') + 2u' \end{aligned} \tag{A.5}$$

$$\begin{aligned}\Lambda_{u5} &= -[w'(-w''' + \theta' v'') + v'\theta' w'']\cos^2\theta - [w'(v''' + 2w''\theta') + v'(w''' - 2\theta' v'')]\cos\theta\sin\theta \\ &\quad + [w'\theta' v'' + v'(v''' + w''\theta')]\sin^2\theta - \frac{1}{4}\theta'^2(-2 + w'^2 + v'^2) \end{aligned} \tag{A.6}$$

$$\Lambda_{v1} = [(v''' + w''\theta')c^2 + (\dot{w}'\theta' + w''\dot{\theta} + 2\dot{v}'')c + \dot{w}'\dot{\theta} + \ddot{v}']j_\zeta - (\dot{\theta} + \theta' c)(\dot{w}' + w''c)j_\eta - (v''' + w''\theta')\beta_\zeta \tag{A.7}$$

$$\begin{aligned}\Lambda_{v2} &= -[(2\theta' v'' - w''')c^2 + 2(\dot{v}'\theta' - \dot{w}'' + v''\dot{\theta})c + 2\dot{v}'\dot{\theta} - \ddot{w}']j_\zeta \\ &\quad - [(w''' - 2\theta' v'')c^2 + 2(-\dot{v}'\theta' + \dot{w}'' - v''\dot{\theta})c - 2\dot{v}'\dot{\theta} + \ddot{w}']j_\eta - (w''' - 2\theta' v'')\beta_\zeta \end{aligned} \tag{A.8}$$

$$\Lambda_{v3} = -(\dot{\theta} + \theta' c)(\dot{w}' + w''c)j_\zeta + [(v''' + w''\theta')c^2 + (\dot{w}'\theta' + 2\dot{v}'' + w''\dot{\theta})c + \dot{w}'\dot{\theta} + \ddot{v}']j_\eta + w''\theta'\beta_\zeta \tag{A.9}$$

$$\Lambda_{v4} = v'\theta'^2\mu\beta_\zeta + 2\mu(-\dot{v}c - v'c^2 + v') + v'^3 + (w'^2 + 2u')v' \tag{A.10}$$

$$\Lambda_{v5} = w''\theta'\cos^2\theta + (w''' - 2v''\theta')\sin\theta\cos\theta + (-v''' - w''\theta')\sin^2\theta + \frac{1}{2}v'\theta'^2 \tag{A.11}$$

$$\Lambda_{w1} = (\dot{\theta} + \theta' c)(\dot{v}' + v''c)j_\zeta + [(w''' - \theta' v'')c^2 + (2\dot{w}'' - \dot{v}'\theta' - v''\dot{\theta})c - \dot{v}'\dot{\theta} + \ddot{w}']j_\eta - v''\theta'\beta_\zeta \tag{A.12}$$

$$\begin{aligned}\Lambda_{w2} &= 2\left[\left(\frac{1}{2}v''' + w''\theta'\right)c^2 + (w''\dot{\theta} + \dot{v}'' + \dot{w}'\theta')c + \dot{w}'\dot{\theta} + \frac{1}{2}\ddot{v}'\right]j_\zeta \\ &\quad - 2\left[\left(\frac{1}{2}v''' + w''\theta'\right)c^2 + (w''\dot{\theta} + \dot{v}'' + \dot{w}'\theta')c + \dot{w}'\dot{\theta} + \frac{1}{2}\ddot{v}'\right]j_\eta - (v''' + 2w''\theta')\beta_\zeta \end{aligned} \tag{A.13}$$

$$\Lambda_{w3} = [(w''' - \theta' v'')c^2 + (-\dot{v}'\theta' + 2\dot{w}'' - v''\dot{\theta})c - \dot{v}'\dot{\theta} + \ddot{w}']j_\zeta + (\dot{\theta} + \theta' c)(\dot{v}' + v''c)j_\eta - (w''' - \theta' v'')\beta_\zeta \tag{A.14}$$

$$\Lambda_{w4} = w'\theta'^2\mu\beta_\zeta + 2\mu(-w'c^2 - c\dot{w} + w') + w'^3 + (2u' + v'^2)w' \tag{A.15}$$

$$\Lambda_{w5} = -(w''' - v''\theta')\cos^2\theta + (v''' + 2w''\theta')\sin\theta\cos\theta - v''\theta'\sin^2\theta + \frac{1}{2}w'\theta'^2 \tag{A.16}$$

$$\Lambda_{\theta1} = -2v''w''\beta_\zeta - 2(j_\eta - j_\zeta)(\dot{w}' + w''c)(\dot{v}' + v''c) \tag{A.17}$$

$$\Lambda_{\theta2} = 2(v''^2 - w''^2)\beta_\zeta + 2[(v'' + w'')c + \dot{v}' + \dot{w}'][(v'' - w'')c + \dot{v}' - \dot{w}'](j_\eta - j_\zeta) \tag{A.18}$$

$$\Lambda_{\theta3} = 2v''w''\beta_\zeta + 2(j_\eta - j_\zeta)(\dot{w}' + w''c)(\dot{v}' + v''c) \tag{A.19}$$

$$\Lambda_{\theta4} = [2w'w''\theta' + 2v'v''\theta' + (2u' + v'^2 + w'^2 + 2\mu)\theta'' + 2u''\theta']\beta_\zeta - 2(\ddot{\theta} + 2\dot{\theta}'c + \theta''c^2)j_\xi + 2\theta''\beta_\xi \tag{A.20}$$

$$\begin{aligned}\Lambda_{\theta5} &= 2v''w''\cos^2\theta - 2(v''^2 - w''^2)\cos\theta\sin\theta - 2v''w''\sin^2\theta + 2w'w''\theta' \\ &\quad + 2v'v''\theta' + (2u' + v'^2 + w'^2 + 2\mu)\theta'' + 2u''\theta' \end{aligned} \tag{A.21}$$

The expressions for the $\widehat{H}_\alpha$ in (50) are

$$\begin{aligned}\widehat{H}_\alpha &= \Pi_{\alpha 1}\cos^2\theta + \Pi_{\alpha 2}\sin\theta\cos\theta + \Pi_{\alpha 3}\sin^2\theta + \Pi_{\alpha 4}\frac{\beta_\zeta}{\beta_\eta}, \quad \alpha = u, v, w \\ \widehat{H}_\theta &= -\left(\beta_\zeta + \frac{\beta_\zeta}{\beta_\eta}\right)\left(u' + \frac{1}{2}v'^2 + \frac{1}{2}w'^2 + \mu\right)\theta' + (\dot{\theta} + \theta' c)j_\xi c - \beta_\xi\theta'\end{aligned} \tag{A.22}$$

where the $\Pi_{\alpha i}$ are

$$\Pi_{u1} = v'v''\beta_\zeta - [v'(\dot{v}' + v''c)j_\zeta + w'(\dot{w}' + w''c)j_\eta]c \tag{A.23}$$

$$\Pi_{u2} = (w'v'' + v'w'')\beta_\zeta + (j_\eta - j_\zeta)[(w'v'' + v'w'')c + v'\dot{w}' + \dot{v}'w']c \tag{A.24}$$

$$\Pi_{u3} = w'w''\beta_\zeta - [w'(\dot{w}' + w''c)j_\zeta + v'(\dot{v}' + v''c)j_\eta]c \tag{A.25}$$

$$\Pi_{u4} = (w'\cos\theta - v'\sin\theta)(-v''\sin\theta + w''\cos\theta) \tag{A.26}$$

$$\Pi_{v1} = -v''\beta_\zeta + (\dot{v}' + v''c)j_\zeta c \tag{A.27}$$

$$\Pi_{v2} = -w''\beta_\zeta - (\dot{w}' + w''c)(j_\eta - j_\zeta)c \tag{A.28}$$

$$\Pi_{v3} = (\dot{v}' + v''c)j_\eta c \tag{A.29}$$

$$\Pi_{v4} = \sin\theta(w''\cos\theta - v''\sin\theta) \tag{A.30}$$

$$\Pi_{w1} = (\dot{w}' + w''c)j_\eta c \tag{A.31}$$

$$\Pi_{w2} = -v''\beta_\zeta - c(j_\eta - j_\zeta)(\dot{v}' + v''c) \tag{A.32}$$

$$\Pi_{w3} = -w''\beta_\zeta + (\dot{w}' + w''c)j_\zeta c \tag{A.33}$$

$$\Pi_{w4} = \cos\theta(-w''\cos\theta + v''\sin\theta) \tag{A.34}$$

References

Crespo da Silva, M.R.M., 1988. Non-linear flexural–flexural–torsional–extensional dynamics of beams—I. Formulation. Int. J. Solids Struct. 24 (12), 1225–1234.

Crespo da Silva, M.R.M., 1991. Equations for nonlinear analysis of 3D motions of beams. Appl. Mech. Rev. 44 (11 Part 2).

Crespo da Silva, M.R.M., Glynn, C.C., 1978. Nonlinear flexural–flexural–torsional dynamics of inextensional beams. I. Equations of motion. J. Struct. Mech. 6 (4), 437–448.

Doedel, E.J., Champneys, A.R., et al., 1997. Auto 97: Continuation and Bifurcation Software for Ordinary Differential Equations (with Homcont).

Hodges, D.H., 2001. Lateral–torsional flutter of a deep cantilever loaded by a lateral follower force at the tip. J. Sound Vib. 247 (1), 175–183.

Hodges, D.H., Peters, D.A., 1975. On the lateral buckling of uniform slender cantilever beams. Int. J. Solids Struct. 11, 1269–1280.

Kong, L., Parker, R.G., 2003. Equilibrium and belt-pulley vibration coupling in serpentine belt drives. ASME J. Appl. Mech. 70 (5), 739–750.

Kong, L., Parker, R.G., 2005. Steady state mechanics of belt-pulley systems. ASME J. Appl. Mech. 75, 25–34.

Love, A.E.H., 1944. A Treatise on the Mathematical Theory of Elasticity. Dover Publications, New York.

Michell, A.G.M., 1899. Elastic stability of long beams under transverse forces. Philos. Mag. 48 (5th Series), 298–309.

Milisavljevic, B.M., 1995. On lateral buckling of a slender cantilever beam. Int. J. Solids Struct. 32 (16), 2377–2391.

Mote Jr., C.D., 1968. Divergence buckling of an edge-loaded axially moving band. Int. J. Mech. Sci. 10, 281–295.

Mote Jr., C.D., Wu, W.Z., 1985. Vibration coupling in continuous belt and band systems. J. Sound Vib. 102, 1–9.

Orloske, K.M., Parker, R.G., this issue. Flexural–torsional buckling of misaligned axially moving beams. II. Vibration and stability analysis. Int. J. Solids Struct., doi:10.1016/j.ijsolstr.2005.08.015.

Pai, P.F., Nayfeh, A.H., 1990. Three-dimensional nonlinear vibrations of composite beams—I. Equations of motion. Nonlinear Dyn. 1, 477–502.

Prandtl, L., 1899. Kipperscheinungen, Dissertation der Universität München.

Raboud, D.W., Faulkner, M.G., Lipsett, A.W., 1996. Multiple three-dimensional equilibrium solutions for cantilever beams loaded by dead tip and uniform distributed loads. Int. J. Non-Linear Mech. 31 (3), 297–311.

Raboud, D.W., Faulkner, M.G., et al., 2001. Stability evaluation of very flexible cantilever beams. Int. J. Non-Linear Mech. 36, 1109–1122.

Reissner, E., 1979. On lateral buckling of end-loaded cantilever beams. ZAMP 30, 31–40.

Ritchie, S.J.K., Leevers, P.S., 1999. Non-uniform and dynamic torsion of elastic beams, Part 1: Governing equations and particular solutions. J. Strain Anal. 34 (5), 303–311.
Timoshenko, S.P., 1936. Theory of Elastic Stability. McGraw-Hill, New York.
Timoshenko, S.P., Goodier, J.N., 1970. Theory of Elasticity. McGraw-Hill, New York.
Trahair, N.S., 1993. Flexural–Torsional Buckling of Structures. CRC Press, Ann Arbor.
Vlasov, V.Z., 1961. Thin-Walled Elastic Beams. Israel Program for Scientific Translation, Jerusalem.
Wang, K.W., Mote Jr., C.D., 1986. Vibration coupling analysis of band/wheel mechanical systems. J. Sound Vib. 109, 237–258.
Wickert, J.A., 1992. Non-linear vibration of a traveling tensioned beam. Int. J. Non-Linear Mech. 27 (3), 503–517.